regions of the cDNA for mouse COX-2 (O'Banion et al. 1992). The β-actin cDNA amplimers were 5′-GTGGGCCGGTCTAGGCACCA-3′ (sense) and 5′-GGTTGGCCTTAGGGTTCAGG-3′ (antisense; Kaartinen et al. 1995). β-actin messenger RNA (mRNA) was assessed to control for the amount and the integrity of RNA in each sample. Each PCR cycle consisted of a denaturation step (94°C for 45 s), an annealing step (60°C for 45 s), and a primer extension step (72°C for 2 min). PCR products were separated by 10% polyacrylamide gel electrophoresis and visualized by ethidium bromide staining. The densities of the bands corresponding to COX-2 and β-actin were analyzed by densitometry (NIH Image J software).

Statistical Analysis

One-way analysis of variance was carried out to determine the levels of significance in experiments. Multiple group comparisons were performed using the Student–Newman–Keuls test. Data are given as means ± SD values.

Results

IL-6 Stimulates PGE_2 Release in Cultured Mouse Astrocytes

Release of PGE_2 into the supernatants of cultured astrocytes was assayed by EIA. The dose-dependent effects of IL-6 were examined by 20-h culturing at concentrations of 0.01 to 10 ng/ml. As shown in Fig. 1a, IL-6 produced a dose-dependent increase in PGE_2 release from astrocytes; the plateau was reached at 1 ng/ml. The increase in PGE_2 release at plateau, which was about 2.5-fold over the control level, was observed at concentrations of 1 and 10 ng/ml. Based on this observation, IL-6 was used at a concentration of 10 ng/ml in further experiments unless stated otherwise. The time-dependent changes in PGE_2 release at a concentration of 10 ng/ml of IL-6 are shown in Fig. 1b. PGE_2 release increased significantly from as early as 8 h in culture and thereafter reached a maximum at 20 h in culture. These results indicate that IL-6 induces PGE_2 release in astrocytes.

IL-6 Induces COX-2 mRNA Expression in Cultured Mouse Astrocytes

To determine the mechanism by which IL-6 increases PGE_2 release into the supernatants of cultured astrocytes, we isolated RNA from astrocytes and subjected it to reverse transcriptase PCR (RT-PCR) analysis using primers for COX-2. Expression of the *β-actin* gene was used as a control for normalization. The RT-PCR analysis of RNA

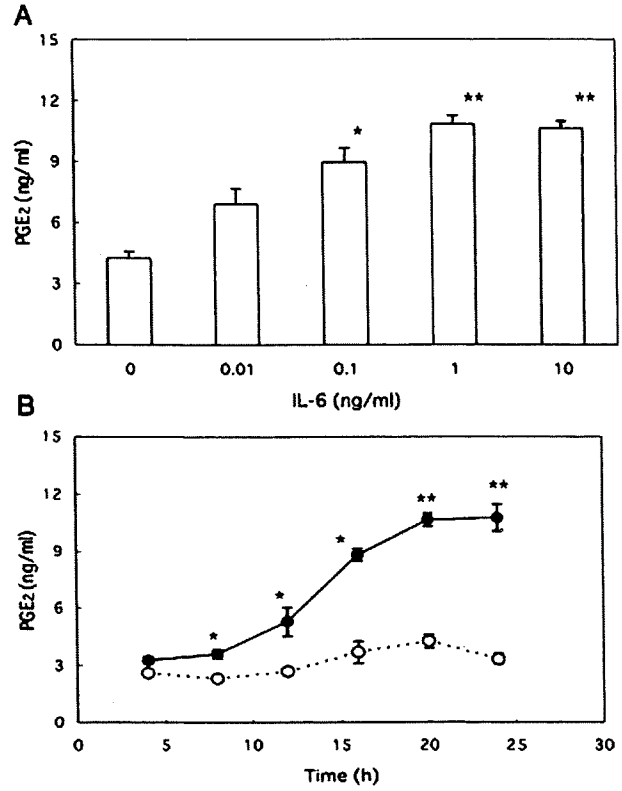

Figure 1 IL-6 induces PGE_2 release in astrocytes. Cells were treated with vehicle as a control or the indicated concentrations of IL-6 for 20 h (**a**). Cells were treated with vehicle as a control (*empty circle*) and 10 ng/ml IL-6 for various times as indicated (*filed circle*) (**b**). After incubation, the culture media were collected and the levels of PGE_2 were measured by EIA. Data are mean ± SD (*bars*) values from five independent experiments. Significant increases in PGE_2 release compared with the control are indicated by *asterisks*: $*p<0.05$, $**p<0.01$

isolated from IL-6-treated astrocytes confirmed that COX-2 mRNA was induced in mouse astrocytes by 10 ng/ml IL-6 (Fig. 2). As shown in Fig. 2, treatment with IL-6 resulted in a time-dependent expression of COX-2 mRNA. COX-2 mRNA levels increased significantly from as early as 1 h in culture and thereafter seemed to be produced at a similar level, namely 2.4-fold above the control level, until 5 h in culture; COX-2 mRNA levels returned to the control level after 6 h in culture. These data indicate that COX-2 mRNA levels are increased in IL-6-stimulated astrocytes.

IL-6 Induces COX-2 Protein Synthesis in Cultured Mouse Astrocytes

A recent study demonstrated that IL-6 mediates COX-2 induction in prostatic intraepithelial neoplasia cells (Liu et al. 2002). Therefore, we examined the effect of IL-6 on COX-2 expression by astrocytes. As shown in Fig. 3,

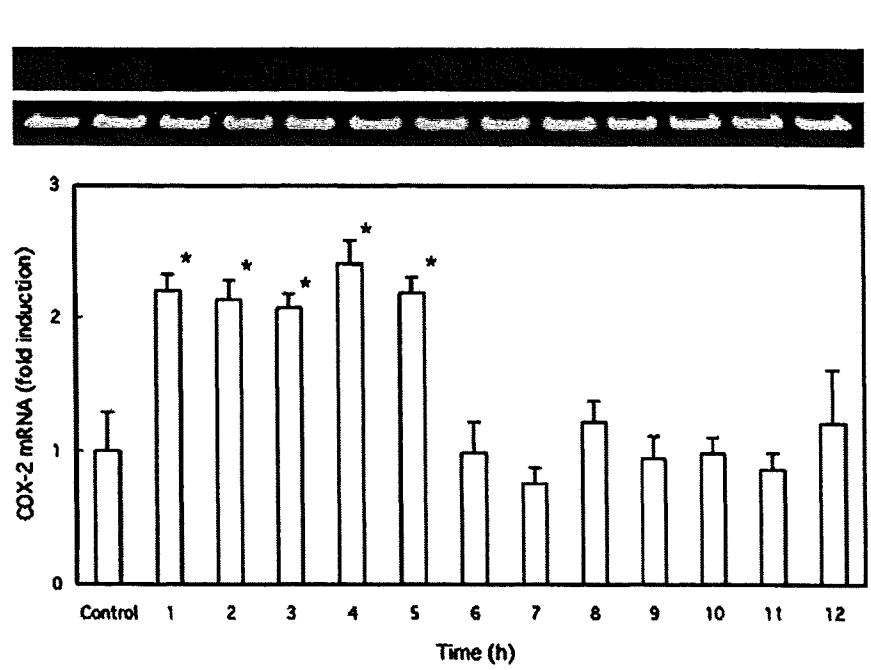

Figure 2 Time course of COX-2 mRNA induction by IL-6 in astrocytes. Cells were treated with 10 ng/ml IL-6 for the indicated times. Total RNA was isolated and the levels of mRNAs for COX-2 and β-actin were determined by RT-PCR (a). Band intensities were analyzed using Image J 1.32 software, and for each sample, COX-2 mRNA levels were normalized to the mRNA levels of the housekeeping *β-actin* gene. Data are mean ± SD (*bars*) values from five independent experiments. Values are expressed as fold induction to control cultures defined as 1.0. Significant increases in COX-2 mRNA induction compared with the control are indicated by *asterisks*: $*p<0.05$ (b)

astrocytes expressed basal levels of COX-2, and this expression was increased in the presence of 10 ng/ml IL-6. The IL-6 induction of COX-2 expression was time-dependent, with a peak increase noted 2 h after IL-6 treatment, and COX-2 expression remained elevated up to 6 h after treatment. COX-2 migrates in this electrophoretic system as a doublet (owing to glycosylation) approximately 70–72 kDa in size (Morham et al. 1995).

Effect of IL-6 in the Absence and Presence of sIL-6R on PGE_2 Release in Cultured Mouse Astrocytes

The receptor mediating the biological activities of IL-6 is composed of two subunits: IL-6R and gp130. Additionally, sIL-6R, with a molecular weight of approximately 50 kDa, was identified as a central element in the mediation of IL-6 signaling (Peters et al. 1998). To determine whether IL-6 could complex with sIL-6R and affect PGE_2 release, astrocytes were incubated with increasing concentrations of sIL-6R and sIL-6R antibodies. Figure 4a shows the effects of IL-6 on PGE_2 production when added in combination with sIL-6R to the culture. When astrocytes were treated with 10 ng/ml IL-6 in the presence of various concentrations of sIL-6R for 24 h, the release of PGE_2 was dependent on the concentration of sIL-6R (0.01–100 ng/ml): the maximum increase in PGE_2 release, which was about 5.3-fold over the control level (17.83±5.52 ng/ml), was observed at a concentration of 100 ng/ml sIL-6R. Figure 4b shows the effects of a neutralizing antibody against human sIL-6R on PGE_2 formation induced by 10 ng/ml IL-6 in a 24-h culture. The human sIL-6R antibody suppressed the PGE_2 formation induced by IL-6 in a dose-dependent manner (0.01–10 μg/ml). The effective suppression of PGE_2 release induced by sIL-6R antibody was observed at concentrations of 1 and 10 μg/ml. These results indicate that IL-6/sIL-6R complexes stimulate PGE_2 release in cultured astrocytes.

Effect of a Neutralizing Antibody against gp130 on PGE_2 Release in Cultured Mouse Astrocytes

The first step in the IL-6 transducing mechanisms is the binding of the cytokine to its specific receptor subunit followed by the association of a second subunit, the signal transducer gp130 (Hibi et al. 1990). To determine whether IL-6-induced PGE_2 release is coupled with gp130, astrocytes were incubated with increasing concentrations of an anti-mouse gp130 antibody. Figure 5 shows the effect of this neutralizing antibody against mouse gp130 on PGE_2 formation induced by IL-6 and sIL-6R in a 24-h culture. As the maximum effect on PGE_2 release induced by IL-6 was observed at a concentration of 1 ng/ml (Fig. 1a), cells were treated with 1 ng/ml IL-6 in the presence of various concentrations of gp130 antibody, with or without 100 ng/ml sIL-6R. The mouse gp130 antibody suppressed the PGE_2 formation induced by IL-6 as well as IL-6/sIL-6R complexes in a dose-dependent manner (0.01–10 μg/ml): the maximum suppressions on PGE_2 release induced by IL-6 and IL-6/sIL-6R complexes, which were about 77.7% and 68.3% compared with the control levels, respectively, were

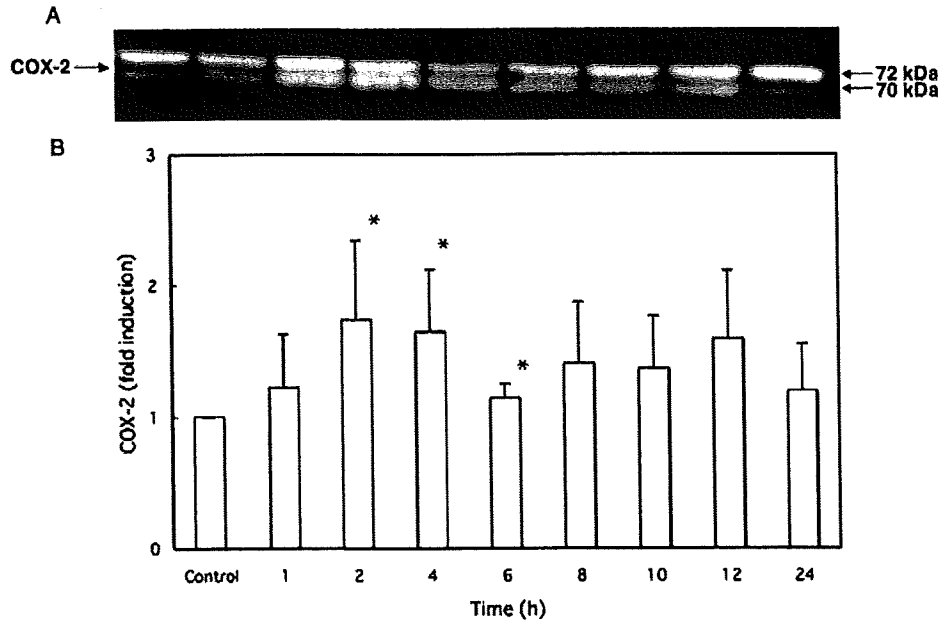

Figure 3 Time course of COX-2 protein induction by IL-6 in astrocytes. Cells were treated with 10 ng/ml IL-6 for the indicated times. Then, cell lysates were prepared and Western blot analysis was performed as described in the "Materials and Methods". A typical Western blot pattern of COX-2 is shown in a. The approximate sizes of glycosylated and unglycosylated COX-2 proteins are indicated on the *right*. A quantitative assay of Western blotting was performed using ImageMaster ID Elite. Data are mean ± SD (*bars*) values from four independent experiments. Values are expressed as fold induction to control cultures defined as 1.0. Significant increases in COX-2 protein induction compared with the control are indicated by *asterisks*: $*p<0.05$

observed in the presence of the gp130 antibody at a concentration of 10 μg/ml. As shown in Fig. 5, treatment with gp130 antibody resulted in a decrease in PGE_2 release at concentrations of 1 and 10 μg/ml in non-treated cells (control). These results may be the effect of the gp130 antibody on other stimulants.

Discussion

Astrocyte activation occurs during immune reactions (Saas et al. 2000), and these activated cells synthesize and release such inflammatory compounds as IL-1β and PGs (Dayton and Major 1996). Inflammation-related events appear to have a significant role in the progression and propagation of the neurodegenerative processes in AD (McGeer et al. 1990) and ALS (Almer et al. 2001). Interestingly, the levels of PGs and/or the enzymes involved in PG production are increased in ALS (Almer et al. 2001) and AD (Stephenson et al. 1996). A role for astrocyte-derived PGs in neuronal cell death has been demonstrated. For example, PGE_2 stimulates astrocytic glutamate release and prevents astrocytes from taking up glutamate (Bezzi et al. 1998; Pasti et al. 2001); the consequent increase in extracellular glutamate is neurotoxic (Drachman and Rothstein 2000). These results suggest that astrocytes (and the substances they release) may be a critical component in the mechanisms underlying neurodegeneration. Astrocytes are a major source of PGs in the CNS. Their ability to produce PGE_2 upon stimulation with several stimulants has been reported. For example, LPS and TGF-β caused a concentration-dependent increase in PGE_2 production in primary cultures of rat astrocytes (Luo et al. 1998; Pistritto et al. 1999). Increased production of PGE_2 after stimulation with IL-1β has also been shown in murine astrocytes (O'Banion et al. 1996). Repovic et al. (2003) demonstrated that oncostatin M synergistically upregulates PGE_2 production induced by the pro-inflammatory mediators IL-1 β, TNF-α, and LPS in astrocytes and astroglioma cells. In this report, we demonstrate that IL-6 increases PGE_2 levels at concentrations of 0.1–10 ng/ml and in time-dependent manners in cultured mouse astrocytes (Fig. 1a, b). Since PGE_2 is freely permeable and cannot be stored intracellularly, the observed rise in PGE_2 level is likely to be due to its de novo synthesis (Smith et al. 2000).

Intracellular PGE_2 synthesis requires three classes of enzymes: phospholipase A_2, COX, and PGE_2 synthase. Each of these enzymes has at least two different isoforms, which may be differently expressed in various cell types. Two COX enzymes have been identified thus far. COX-1 is constitutively expressed and largely responsible for baseline prostaglandin production (DeWitt and Smith 1988). COX-2

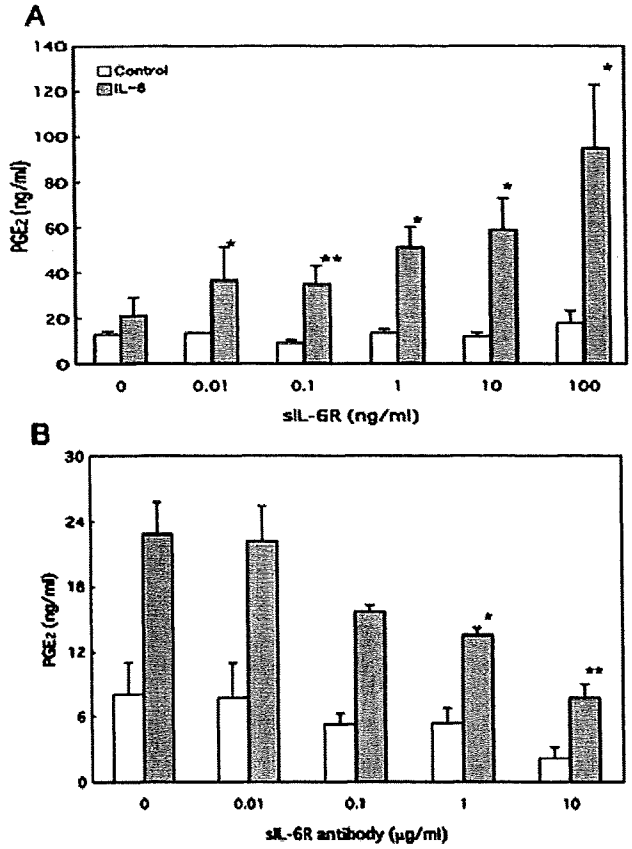

Figure 4 PGE_2 induction by IL-6 in the presence of sIL-6R in astrocytes. Cells were treated with vehicle as a control or 10 ng/ml IL-6 in the presence of various concentrations of sIL-6R (**a**) or sIL-6R antibody (**b**) for 24 h. After incubation, the culture media were collected and the levels of PGE_2 were measured by EIA. Data are mean ± SD (*bars*) values from five independent experiments. Significant increases in PGE_2 release compared with the control are indicated by *asterisks* (**a**); significant decreases in PGE_2 release compared with unstimulated cells are also indicated by *asterisks* (**b**): $*p<0.05$, $**p<0.01$

is the major inducible form of COX and is associated with delayed prostaglandin production (Xie et al. 1991; Kudo and Murakami 1999). In mouse astrocytes treated with IL-6, COX-2 mRNA and protein levels are highly upregulated in medium supplemented with 10% FBS (Figs. 2 and 3). Thus, IL-6-enhanced PGE_2 production is mediated by the stimulatory effect of IL-6 on the expression of COX-2. The present report confirms the results of other studies (Luo et al. 1998; Repovic et al. 2003; Xu et al. 2003) by showing that cultured astrocytes express the inducible COX and secrete PGE_2. On the other hand, O'Banion et al. (1996) demonstrated that IL-1β and phorbol 12-myristate 13-acetate, as well as LPS, TNF-α, and basic fibroblast growth factor (bFGF), but not IL-6, caused a significant accumulation of COX-2 mRNA in astrocytes cultured in serum-free medium. A possible explanation for this discrepancy is as follows. The production of PGs is affected by the serum content of the medium. For example, in osteoblasts and vascular smooth myocytes, serum induces a rapid increase in the expression level of COX-2, but has little effect on COX-1 expression (Pilbeam et al. 1993; Pritchard et al. 1994). FBS contains various mitogenic growth factors, such as bFGF, epidermal growth factor, insulin-like growth factor, and platelet-derived growth factor (PDGF). PDGF can upregulate the mRNA for COX in fibroblasts (Lin et al. 1989). Thus, it is conceivable that these mitogenic growth factors mediate the increase in the expression level of COX-2.

In this report, by 5-h culture, the time needed for maximal expression of COX-2, there was no PGE_2 synthesis. On the other hand, at the time point where PGE_2 is detected (8–24 h culture), there is no COX-2 expression (Figs. 1 and 2). A possible explanation for this discrepancy is as follows. In mammalian cells, prostaglandin-biosynthetic pathways utilizing endogenous arachidonic acid are subdivided into three distinct phases which show different kinetics and possible recruitment of different sets of biosynthetic enzymes. The constitutive immediate response, which occurs within several minutes after stimuli causing a rapid and transient increase in cytoplasmic Ca^{2+}, is regulated by posttranslational activation of constitutively expressed enzymes. The delayed response, which proceeds gradually for several hours after pro-inflammatory stimuli, requires de novo synthesis of particular biosynthetic enzymes. The induced immediate response, which is elicited by Ca^{2+}-mobilizing stimuli after priming by pro-inflammatory stimuli, reflects the combination of the above two responses and involves both

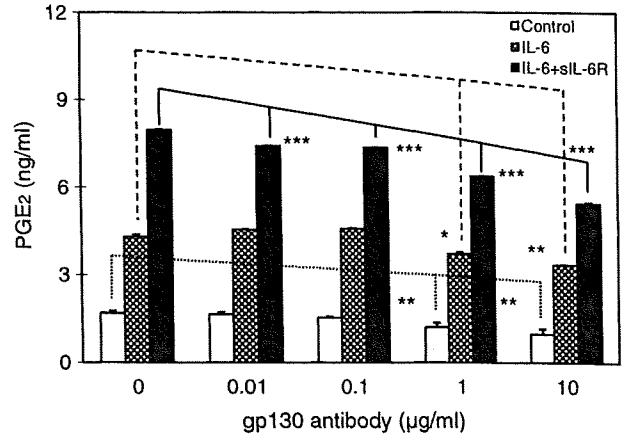

Figure 5 Participation of gp130 in the induction of PGE_2 expression in astrocytes. Cells were treated with 1 ng/ml IL-6 in the presence of various concentrations of gp130 antibody, with or without 100 ng /ml sIL-6R for 24 h. After incubation, the culture media were collected and the levels of PGE_2 were measured by EIA. Data are mean ± SD (*bars*) values from four independent experiments. Significant increases in PGE_2 release compared with the control are indicated by asterisks: $*p<0.05$, $**p<0.01$, $***p<0.001$

constitutive and inducible enzymes. For example, rat peritoneal macrophages treated with LPS predominantly produced PGE_2 during culture for 6–24 h by the delayed response. Delayed PGE_2 generation was accompanied by increasing expression of cytosolic phospholipase A_2 ($cPLA_2$) and de novo induction of COX-2. In the delayed response, $cPLA_2$ and type IIA secretory phospholipase A_2 function cooperatively with inducible COX-2, which was in turn coupled with PGE_2 synthase. COX-1 was non-functional in the delayed response, even though it was constitutively expressed in the cell (Kudo and Murakami 1999). In mouse astrocytes treated with IL-6, PGE_2 synthesis may be regulated by the delayed response.

Cells responsive to IL-6 express on their surface a low affinity receptor that does not have transducing activity. The IL-6/IL-6R complexes induces the homodimerization of a signal-transducing component, gp130, leading to cytoplasmic signaling cascades that activate components of the Janus kinase (JAK)/signal transducers and activators of transcription (STAT) pathway, particularly the activation of the transcription factor STAT-3 (Taga and Kishimoto 1997). sIL-6R can be generated by shedding of the membrane-bound receptor (Mullberg et al. 1993, 1994) or by alternative splicing of mRNA (Lust et al. 1992). Since the transmembrane and cytoplasmic regions of the IL-6R are not essential for signal transduction, sIL-6R can form a complex with IL-6 in solution and associate with gp130, thereby activating signal transduction. Previously, Oh et al. (1998) showed that human astrocytes express low levels of IL-6R and require the addition of sIL-6R for IL-6-mediated responses. Herein, we have shown that treatment of murine astrocytes with IL-6 and sIL-6R leads to marked induction of PGE_2 synthesis, and this effect was suppressed by adding a neutralizing antibody against sIL-6R (Fig. 4). These results suggest that sIL-6R plays a pivotal role in determining the level of PGE_2 synthesis by astrocytes in the CNS and furthermore influences IL-6 function in the CNS. This is supported by several reports that CNS cells that are normally slightly responsive or unresponsive to IL-6 become responsive on addition of sIL-6R. In human astrocytes, IL-6 alone has no effect on α_1-antichymotrypsin expression, whereas addition of sIL-6R leads to its expression (Kordula et al. 1998). In the presence of sIL-6R, IL-6 inhibits TNF-α-induced VCAM-1 expression in astrocytes (Oh et al. 1998). These findings suggest that sIL-6R is a functionally relevant CNS molecule. It is not clear if addition of a neutralizing antibody against sIL-6R to sIL-6R will have any effect on IL-6-induced stimulation of PGE_2 synthesis where exogenous sIL-6R is not added. However, Fig. 4a, b indicates that IL-6/sIL-6R complexes stimulate PGE_2 release in cultured mouse astrocytes.

Gp130, a protein associated with the IL-6/sIL-6R complexes, is a signal-transducing receptor shared by members of the IL-6 cytokine family comprising IL-6, interleukin-11, leukemia inhibitory factor, oncostatin M, ciliary neurotrophic factor, and cardiotrophin-1 (Taga and Kishimoto 1997). The JAK/STAT pathway, an important signal pathway downstream of gp130, has been implicated in diverse pathophysiological processes such as ischemia (Justicia et al. 2000; Choi et al. 2003a, b), inflammation associated with astroglial activation (Gautron et al. 2002), and seizures (Choi et al. 2003a, b; Rosell et al. 2003). Whether increases in gp130-associated STAT3 expression after such a variety of perturbations contribute to subsequent cell death or survival is not fully understood. Numerous studies demonstrate that IL-6 exerts multiple effects, both beneficial and destructive, on CNS cells. In glial cells, IL-6 promotes astrocyte proliferation and is believed to be involved in astrogliosis (Van Wagoner and Benveniste 1999). The present study provided evidence that the mouse gp130 antibody suppressed the PGE_2 formation induced by IL-6 as well as IL-6/sIL-6R complexes in a dose-dependent manner (Fig. 5), suggesting that the IL-6/sIL-6R/gp130 system can modulate the function of PGE_2 synthesis in astrocytes.

Although the precise mechanism underlying induction of PGE_2 synthesis by IL-6 has not yet been elucidated, IL-6/sIL-6R and the signal transducer gp130 play important roles in the regulation of COX-2 expression and subsequent PGE_2 formation in mouse astrocytes, and IL-6 is an important regulator of immune and inflammatory processes in the CNS.

Acknowledgments We are very grateful to Dr. Akira Tanaka for his valuable and helpful advice on the experiments and manuscript preparation.

References

Almer, G., Guegan, C., Teismann, P., et al. (2001). Increased expression of the pro-inflammatory enzyme cyclooxygenase-2 in amyotrophic lateral sclerosis. *Annals of Neurology, 49*, 176–185. doi:10.1002/1531-8249(20010201)49:2<176::AID-ANA37>3.0.CO;2-X.

Bauer, M. K. A., Lieb, K., Schulze-Osthoff, K., et al. (1997). Expression and regulation of cyclooxygenase-2 in rat microglia. *European Journal of Biochemistry, 243*, 726–731. doi:10.1111/j.1432-1033.1997.00726.x.

Bezzi, P., Carmignoto, G., Pasti, L., et al. (1998). Prostaglandins stimulate calcium-dependent glutamate release in astrocytes. *Nature, 391*, 281–285. doi:10.1038/34651.

Bishai, I., & Coceani, F. (1992). Eicosanoid formation in the rat cerebral cortex. *Molecular and Chemical Neuropathology, 17*, 219–238.

Bradford, M. M. (1976). A rapid and sensitive method for the quantitation of microgram quantities of protein utilizing the principle of protein-dye binding. *Analytical Biochemistry, 72*, 248–254. doi:10.1016/0003-2697(76)90527-3.

Choi, J. -S., Kim, S. Y., Cha, J. -H., et al. (2003a). Upregulation of gp130 and STAT3 activation in the rat hippocampus following

transient forebrain ischemia. *Glia, 41*, 237–246. doi:10.1002/glia.10186.

Choi, J. -S., Kim, S. Y., Park, H. -J., et al. (2003b). Upregulation of gp130 and differential activation of STAT and p42/44 MAPK in the rat hippocampus following kainic acid-induced seizures. *Brain Research. Molecular Brain Research, 119*, 10–18. doi:10.1016/j.molbrainres.2003.08.010.

Dayton, E. T., & Major, E. O. (1996). Recombinant human interleukin 1β induces production of prostaglandins in primary human fetal astrocytes and immortalized human fetal astrocyte cultures. *Journal of Neuroimmunology, 71*, 11–18. doi:10.1016/S0165-5728(96)00111-7.

DeWitt, D. L., & Smith, W. L. (1988). Primary structure of prostaglandin G/H synthase from sheep vesicular gland determined from the complementary DNA sequence. *Proceedings of the National Academy of Sciences of the United States of America, 85*, 1412–1416. doi:10.1073/pnas.85.5.1412.

Drachman, D. B., & Rothstein, J. D. (2000). Inhibition of cyclooxygenase-2 protects motor neurons in an organotypic model of amyotrophic lateral sclerosis. *Annals of Neurology, 48*, 792–795. doi:10.1002/1531-8249(200011)48:5<792::AID-ANA14>3.0.CO;2-5.

Dubois, R. N., Abramson, S. B., Crofford, L., et al. (1998). Cyclooxygenase in biology and disease. *The FASEB Journal, 12*, 1063–1073.

Fontana, A., Kristensen, F., Dubs, R., Gemsa, D., & Weber, E. (1982). Production of prostaglandin E and an interleukin-1 like factor by cultured astrocytes and C_6 glioma cells. *Journal of Immunology (Baltimore, MD.: 1950), 129*, 2413–2419.

Gadient, R. A., & Otten, U. (1994). Identification of interleukin-6(IL-6)-expressing neurons in the cerebellum and hippocampus of normal adult rats. *Neuroscience Letters, 182*, 243–246. doi:10.1016/0304-3940(94)90807-9.

Gautron, L., Lafon, P., Chaigniau, M., Tramu, G., & Laye, S. (2002). Spatiotemporal analysis of signal transducer and activator of transcription 3 activation in rat brain astrocytes and pituitary following peripheral immune challenge. *Neuroscience, 112*, 717–729. doi:10.1016/S0306-4522(02)00115-X.

Hayaishi, O. (1991). Molecular mechanisms of sleep-wake regulation: Roles of prostaglandins D_2 and E_2. *The FASEB Journal, 5*, 2575–2581.

Heinrich, P. C., Behrmann, I., Muller-Newen, G., Schaper, F., & Graeve, L. (1998). Interleukin-6-type cytokine signalling through the gp130/Jak/STAT pathway. *The Biochemical Journal, 334*, 297–314.

Hibi, M., Murakami, M., Saito, M., Hirano, T., Taga, T., & Kishimoto, T. (1990). Molecular cloning and expression of an IL-6 signal transducer, gp130. *Cell, 63*, 1149–1157. doi:10.1016/0092-8674(90)90411-7.

Ishimoto, H., Nakahata, N., Matsuoka, I., & Nakanishi, H. (1997). Effects of ATP on phosphoinositide hydrolysis and prostaglandin E_2 generation in rabbit astrocytes. *The Journal of Pharmacy and Pharmacology, 49*, 520–524.

Jacobs, T. P., Shohami, E., Baze, W., et al. (1987). Deteriorating stroke model: Histopathology, edema, and eicosanoid changes following spinal cord ischemia in rabbits. *Stroke, 18*, 741–750.

Justicia, C., Gabriel, C., & Planas, A. M. (2000). Activation of the JAK/STAT pathway following transient focal cerebral ischemia: Signaling through Jak1 and Stat3 in astrocytes. *Glia, 30*, 253–270. doi:10.1002/(SICI)1098-1136(200005)30:3<253::AID-GLIA5>3.0.CO;2-O.

Kaartinen, V., Voncken, J. W., Shuler, C., et al. (1995). Abnormal lung development and cleft palate in mice lacking TGF-β3 indicates defects of epithelial-mesenchymal interaction. *Nature Genetics, 11*, 415–421. doi:10.1038/ng1295-415.

Kishimoto, T., Taga, T., & Akira, S. (1994). Cytokine signal transduction. *Cell, 76*, 253–262. doi:10.1016/0092-8674(94)90333-6.

Kordula, T., Rydel, R. E., Brigham, E. F., Horn, F., Heinrich, P. C., & Travis, J. (1998). Oncostatin M and the interleukin-6 and soluble interleukin-6 receptor complex regulate α_1-antichymotrypsin expression in human cortical astrocytes. *The Journal of Biological Chemistry, 273*, 4112–4118. doi:10.1074/jbc.273.7.4112.

Kudo, I., & Murakami, M. (1999). Diverse functional coupling of prostanoid biosynthetic enzymes in various cell types. *Advances in Experimental Medicine and Biology, 469*, 29–35.

Lin, A. H., Bienkowski, M. J., & Gorman, R. R. (1989). Regulation of prostaglandin H synthase mRNA levels and prostaglandin biosynthesis by platelet-derived growth factor. *The Journal of Biological Chemistry, 264*, 17379–17383.

Liu, X. -H., Kirschenbaum, A., Lu, M., et al. (2002). Prostaglandin E_2 stimulates prostatic intraepithelial neoplasia cell growth through activation of the interleukin-6/gp130/Stat-3 signaling pathway. *Biochemical and Biophysical Research Communications, 290*, 249–255. doi:10.1006/bbrc.2001.6188.

Luo, J., Lang, J. A., & Miller, M. W. (1998). Transforming growth factor β1 regulates the expression of cyclooxygenase in cultured cortical astrocytes and neurons. *Journal of Neurochemistry, 71*, 526–534.

Lust, J. A., Donovan, K. A., Kline, M. P., Greipp, P. R., Kyle, R. A., & Maihle, N. J. (1992). Isolation of an mRNA encoding a soluble form of the human interleukin-6 receptor. *Cytokine, 4*, 96–100. doi:10.1016/1043-4666(92)90043-Q.

Marcheselli, V. L., & Bazan, N. G. (1996). Sustained induction of prostaglandin endoperoxide synthetase-2 by seizures in hippocampus. *The Journal of Biological Chemistry, 271*, 24794–24799. doi:10.1074/jbc.271.40.24794.

Marz, P., Cheng, J. G., Gadient, R. A., et al. (1998). Sympathetic neurons can produce and respond to interleukin 6. *Proceedings of the National Academy of Sciences of the United States of America, 95*, 3251–3256. doi:10.1073/pnas.95.6.3251.

McGeer, P. L., McGeer, E., Rogers, J., & Sibley, J. (1990). Anti-inflammatory drugs and Alzheimer disease. *Lancet, 335*, 1037. doi:10.1016/0140-6736(90)91101-F.

Minghetti, L., & Levi, G. (1995). Induction of prostanoid biosynthesis by bacterial lipopolysaccharide and isoproterenol in rat microglial cultures. *Journal of Neurochemistry, 65*, 2690–2698.

Minghetti, L., Walsh, D. T., Levi, G., & Perry, V. H. (1999). In vivo expression of cyclooxygenase-2 in rat brain following intraparenchymal injection of bacterial endotoxin and inflammatory cytokines. *Journal of Neuropathology and Experimental Neurology, 58*, 1184–1191. doi:10.1097/00005072-199911000-00008.

Molina-Holgado, E., Ortiz, S., Molina-Holgado, F., & Guaza, C. (2000). Induction of COX-2 and PGE_2 biosynthesis by IL-1β is mediated by PKC and mitogen-activated protein kinases in murine astrocytes. *British Journal of Pharmacology, 131*, 152–159. doi:10.1038/sj.bjp.0703557.

Mollace, V., Colasanti, M., Muscoli, C., et al. (1998). The effect of nitric oxide on cytokine-induced release of PGE_2 by human cultured astroglial cells. *British Journal of Pharmacology, 124*, 742–746. doi:10.1038/sj.bjp.0701852.

Montine, T. J., Sidell, K. R., Crews, B. C., et al. (1999). Elevated CSF prostaglandin E_2 levels in patients with probable AD. *Neurology, 53*, 1495–1498.

Morham, S. G., Langenbach, R., Loftin, C. D., et al. (1995). Prostaglandin synthase 2 gene disruption causes severe renal pathology in the mouse. *Cell, 83*, 473–482. doi:10.1016/0092-8674(95)90125-6.

Mullberg, J., Schooltink, H., Stoyan, T., et al. (1993). The soluble interleukin-6 receptor is generated by shedding. *European Journal of Immunology, 23*, 473–480. doi:10.1002/eji.1830230226.

Mullberg, J., Oberthur, W., Lottspeich, F., et al. (1994). The soluble human IL-6 receptor: Mutational characterization of the proteo-

lytic cleavage site. *Journal of Immunology (Baltimore, MD.: 1950), 152*, 4958–4968.

Nogawa, S., Zhang, F., Ross, M. E., & Iadecola, C. (1997). Cyclo-oxygenase-2 gene expression in neurons contributes to ischemic brain damage. *The Journal of Neuroscience, 17*, 2746–2755.

O'Banion, M. K., Winn, V. D., & Young, D. A. (1992). cDNA cloning and functional activity of a glucocorticoid-regulated inflammatory cyclooxygenase. *Proceedings of the National Academy of Sciences of the United States of America, 89*, 4888–4892. doi:10.1073/pnas.89.11.4888.

O'Banion, M. K., Miller, J. C., Chang, J. W., Kaplan, M. D., & Coleman, P. D. (1996). Interleukin-1β induces prostaglandin G/H synthase-2 (cyclooxygenase-2) in primary murine astrocyte cultures. *Journal of Neurochemistry, 66*, 2532–2540.

Oh, J. -W., Wagoner, N. J. V., Rose-John, S., & Benveniste, E. N. (1998). Role of IL-6 and the soluble IL-6 receptor in inhibition of VCAM-1 gene expression. *Journal of Immunology (Baltimore, MD.: 1950), 161*, 4992–4999.

Pasti, L., Zonta, M., Pozzan, T., Vicini, S., & Carmignoto, G. (2001). Cytosolic calcium oscillations in astrocytes may regulate exocytotic release of glutamate. *The Journal of Neuroscience, 21*, 477–484.

Peters, M., Muller, A. M., & Rose-John, S. (1998). Interleukin-6 and soluble interleukin-6 receptor: direct stimulation of gp130 and hematopoiesis. *Blood, 92*, 3495–3504.

Pilbeam, C. C., Kawaguchi, H., Hakeda, Y., Voznesensky, O., Alander, C. B., & Raisz, L. G. (1993). Differential regulation of inducible and constitutive prostaglandin endoperoxide synthase in osteoblastic MC3T3-E1 cells. *The Journal of Biological Chemistry, 268*, 25643–25649.

Pistritto, G., Mancuso, C., Tringali, G., Perretti, M., Preziosi, P., & Navarra, P. (1998). The relative contribution of constitutive and inducible cyclooxygenase activity to lipopolysaccharide-induced prostaglandin production by primary cultures of rat hypothalamic astrocytes. *Neuroscience Letters, 246*, 45–48. doi:10.1016/S0304-3940(98)00226-2.

Pistritto, G., Franzese, O., Pozzoli, G., et al. (1999). Bacterial lipopolysaccharide increases prostaglandin production by rat astrocytes via inducible cyclo-oxygenase: Evidence for the involvement of nuclear factor κB. *Biochemical and Biophysical Research Communications, 263*, 570–574. doi:10.1006/bbrc.1999.1413.

Pritchard, K. A., O'Banion, M. K., Miano, J. M., et al. (1994). Induction of cyclooxygenase-2 in rat vascular smooth muscle cells in vitro and in vivo. *The Journal of Biological Chemistry, 269*, 8504–8509.

Repovic, P., Mi, K., & Benveniste, E. N. (2003). Oncostatin M enhances the expression of prostaglandin E_2 and cyclooxygenase-2 in astrocytes: Synergy with interleukin-1β, tumor necrosis factor-α, and bacterial lipopolysaccharide. *Glia, 42*, 433–446. doi:10.1002/glia.10182.

Rose-John, S., & Heinrich, P. C. (1994). Soluble receptors for cytokines and growth factors: generation and biological function. *The Biochemical Journal, 300*, 281–290.

Rosell, D. R., Akama, K. T., Nacher, J., & McEwen, B. S. (2003). Differential expression of suppressors of cytokine signaling-1, -2, and -3 in the rat hippocampus after seizure: Implications for neuromodulation by gp130 cytokines. *Neuroscience, 122*, 349–358. doi:10.1016/S0306-4522(03)00594-3.

Saas, P., Boucraut, J., Walker, P. R., et al. (2000). TWEAK stimulation of astrocytes and the proinflammatory consequences. *Glia, 32*, 102–107. doi:10.1002/1098-1136(200010)32:1<102::AID-GLIA100>3.0.CO;2-U.

Samad, T. A., Moore, K. A., Sapirstein, A., et al. (2001). Interleukin 1β-mediated induction of cox-2 in the CNS contributes to inflammatory pain hypersensitivity. *Nature, 410*, 471–475. doi:10.1038/35068566.

Sawada, M., Suzumura, A., Ohno, K., & Marunouchi, T. (1993). Regulation of astrocyte proliferation by prostaglandin E_2 and the α subtype of protein kinase C. *Brain Research, 613*, 67–73. doi:10.1016/0006-8993(93)90455-V.

Sawada, M., Suzumura, A., & Marunouchi, T. (1995). Cytokine network in the central nervous system and its roles in growth and differentiation of glial and neuronal cells. *International Journal of Developmental Neuroscience, 13*, 253–264. doi:10.1016/0736-5748(94)00076-F.

Seregi, A., Keller, M., Jackisch, R., & Hertting, G. (1984). Comparison of the prostanoid synthesizing capacity in homogenates from primary neuronal and astroglial cell cultures. *Biochemical Pharmacology, 33*, 3315–3318. doi:10.1016/0006-2952(84)90099-6.

Smith, W. L., Garavito, R. M., & DeWitt, D. L. (1996). Prostaglandin endoperoxide H synthases(cyclooxygenases)-1 and -2. *The Journal of Biological Chemistry, 271*, 33157–33160. doi:10.1074/jbc.271.52.33157.

Smith, W. L., DeWitt, D. L., & Garavito, R. M. (2000). Cyclooxygenases: Structural, cellular, and molecular biology. *Annual Review of Biochemistry, 69*, 145–182. doi:10.1146/annurev.biochem.69.1.145.

Stephenson, D. T., Lemere, C. A., Selkoe, D. J., & Clemens, J. A. (1996). Cytosolic phospholipase A_2(cPLA$_2$) immunoreactivity is elevated in Alzheimer's disease brain. *Neurobiology of Disease, 3*, 51–63. doi:10.1006/nbdi.1996.0005.

Taga, T., & Kishimoto, T. (1997). Gp130 and the interleukin-6 family of cytokines. *Annual Review of Immunology, 15*, 797–819. doi:10.1146/annurev.immunol.15.1.797.

Teather, L. A., Lee, R. K. K., & Wurtman, R. J. (2002). Platelet-activating factor increases prostaglandin E_2 release from astrocyte-enriched cortical cell cultures. *Brain Research, 946*, 87–95. doi:10.1016/S0006-8993(02)02866-4.

Their, M., Marz, P., Otten, U., Weis, J., & Rose-John, S. (1999). Interleukin-6(IL-6) and its soluble receptor support survival of sensory neurons. *Journal of Neuroscience Research, 55*, 411–422. doi:10.1002/(SICI)1097-4547(19990215)55:4<411::AID-JNR2>3.0.CO;2-D.

Ushikubi, F., Segi, E., Sugimoto, Y., et al. (1998). Impaired febrile response in mice lacking the prostaglandin E receptor subtype EP_3. *Nature, 395*, 281–284. doi:10.1038/26233.

Van Wagoner, N. J., & Benveniste, E. N. (1999). Interleukin-6 expression and regulation in astrocytes. *Journal of Neuroimmunology, 100*, 124–139. doi:10.1016/S0165-5728(99)00187-3.

Vane, J. R., Bakhle, Y. S., & Botting, R. M. (1998). Cyclooxygenases 1 and 2. *Annual Review of Pharmacology and Toxicology, 38*, 97–120. doi:10.1146/annurev.pharmtox.38.1.97.

Xie, W., Chipman, J. G., Robertson, D. L., Erikson, R. L., & Simmons, D. L. (1991). Expression of a mitogen-responsive gene encoding prostaglandin synthase is regulated by mRNA splicing. *Proceedings of the National Academy of Sciences of the United States of America, 88*, 2692–2696. doi:10.1073/pnas.88.7.2692.

Xu, J., Chalimoniuk, M., Shu, Y., et al. (2003). Prostaglandin E_2 production in astrocytes: Regulation by cytokines, extracellular ATP, and oxidative agents. *Prostaglandins, Leukotrienes, and Essential Fatty Acids, 69*, 437–448. doi:10.1016/j.plefa.2003.08.016.

Yamagata, K., Andreasson, K. I., Kaufmann, W. E., Barnes, C. A., & Worley, P. F. (1993). Expression of a mitogen-inducible cyclooxygenase in brain neurons: Regulation by synaptic activity and glucocorticoids. *Neuron, 11*, 371–386.

Biochemical and Biophysical Research Communications 388 (2009) 589–594

Contents lists available at ScienceDirect

Biochemical and Biophysical Research Communications

journal homepage: www.elsevier.com/locate/ybbrc

Ferritin reporter used for gene expression imaging by magnetic resonance

Kenji Ono, Kazuya Fuma, Kaori Tabata, Makoto Sawada *

Department of Brain Functions, Division of Stress Adaptation and Protection, Research Institute of Environmental Medicine, Nagoya University, Nagoya, Aichi 464-8601, Japan

ARTICLE INFO

Article history:
Received 3 August 2009
Available online 14 August 2009

Keywords:
Magnetic resonance imaging
Optical imaging
Gene expression
Glioma

ABSTRACT

Magnetic resonance imaging (MRI) is a minimally invasive way to provide high spatial resolution tomograms. However, MRI has been considered to be useless for gene expression imaging compared to optical imaging. In this study, we used a ferritin reporter, binding with biogenic iron, to make it a powerful tool for gene expression imaging in MRI studies. GL261 mouse glioma cells were over-expressed with dual-reporter ferritin–DsRed under β-actin promoter, then gene expression was observed by optical imaging and MRI in a brain tumor model. GL261 cells expressing ferritin–DsRed fusion protein showed enhanced visualizing effect by reducing T2-weighted signal intensity for *in vitro* and *in vivo* MRI studies, as well as DsRed fluorescence for optical imaging. Furthermore, a higher contrast was achieved on T2-weighted images when permeating the plasma membrane of ferritin–DsRed-expressing GL261. Thus, a ferritin expression vector can be used as an MRI reporter to monitor *in vivo* gene expression.

Introduction

Magnetic resonance imaging (MRI) is one of the minimally invasive imaging techniques for high spatial resolution tomograms providing anatomical and functional information. Other tomographic imaging techniques like computed tomography (CT) and positron emission tomography (PET) generally entails radiation exposure, unlike MRI, which is free from radiation exposure. Therefore, MRI is accepted as a safer imaging technique compared to others, though it is unsuitable for visualization of gene expression. As a result, optical imaging is generally used for this purpose because several fluorescent and chemiluminescent reporters such as GFP and DsRed and luciferase enzyme systems are available [1]. The availability of gene products capable of altering local signals of MRI for contrast, will be a useful MRI reporter for gene expression.

Iron derivatives are common MRI contrast agents that decrease signal intensity on T2-weighted images as a result of the magnetic susceptibility effect [2]. Thus, localized accumulation of iron derivates are detected by MRI [3]. In fact, iron derivates such as ferumoxides and ferric ammonium citrate are useful in clinical diagnosis of liver neoplasm [4] and gastrointestinal tract [5], respectively. Recent studies suggest use of genes encoding iron-binding proteins as a potential candidate of MRI reporter for *in vivo* MRI detection of gene expression [6].

Ferritin, an endogenous iron storage metalloprotein, consists of 24 light and heavy polypeptide chains encapsulating an iron oxide core with up to 4500 iron atoms [7]. Heavy chain of ferritin mainly binds to iron oxide [8]. Ferritin further creates magnetic fields that affect relaxation time of water protons diffusing through the magnetic field [9]. This makes heavy chain of ferritin an ideal MRI reporter for *in vivo* gene expression in MRI studies.

In this study, we designed a vector capable of expressing heavy chain of ferritin and DsRed fusion protein (ferritin–DsRed) under a β-actin promoter, and made ferritin–DsRed-overexpressing GL261 cell mouse clonal glioma cells, to detect the cells by *in vivo* and *in vitro* magnetic resonance imaging. Results of this study suggest that this ferritin reporter system was useful to detect *in vivo* gene expression by MRI.

Materials and methods

Cell lines. Murine GL261 glioma cells including DsRed expressing and ferritin–DsRed-expressing derivatives were cultured in Dulbecco's Modified Eagle's Medium (DMEM) (Sigma–Aldrich, St. Louis, MO, USA) with 10% fetal bovine serum and Penicillin–Streptomycin (Invitrogen, Carlsbad, CA, USA). Cells were regularly photographed under a fluorescent microscope (IX-70, Olympus, Tokyo, Japan).

Plasmids and electroporation. pferritin–DsRed plasmids were made from a pDsRed-N1 vector (CLONTECH Laboratories, Inc., Mountain View, CA, USA) by insertion of a mouse heavy chain of ferritin sequence (NM_010239). The mouse heavy chain of ferritin sequence was amplified by polymerase chain reaction, then PCR products were treated with restriction enzymes, HindIII and BamHI, and ligated into the pDsRed-N1 vector at the multi-cloning site. GL261 cells (1×10^6 cells/400 μl) were mixed with 10 μg of the

* Corresponding author. Fax: +81 52 789 3994.
E-mail address: msawada@riem.nagoya-u.ac.jp (M. Sawada).

0006-291X/$ - see front matter © 2009 Elsevier Inc. All rights reserved.
doi:10.1016/j.bbrc.2009.08.055

plasmids in a 4 mm gap cuvette. The cuvette was set in an ECM830 electroporator (BTX Instrument Division Harvard Apparatus, Inc., Holliston, MA, USA) and electroporation was performed under the following condition (Choose mode: LV mode, Set Voltage: 170 V, Set Pulse Length: 70 ms, Set Number of Pulses: 1). Electroporated cells were cultured in the medium with 400 μg/ml of G418 for selection of mixed clone expressed ferritin–DsRed for 7 days.

RNA extraction and RT-PCR. Total RNA was extracted from cells using RNeasy Mini kit and RNase-free DNase set (QIAGEN, Hilden, Germany) according to the manufacturer's instruction. RNA (1 μg) was reverse transcribed at 37 °C for 90 min in a mixture containing 100 U of recombinant M-MLV reverse transcriptase, 0.1 μg DNA random hexamers, 40 U RNase inhibitor and 1.4 mM dNTPs, in a final volume of 50 μl. The cDNA was amplified with *Taq* DNA polymerase (Takara, Tokyo, Japan), using primer pairs specific to DsRed (sense primer: TTC CAG TAC GGC TCC AAG GT; antisense primer: GAG GAG TCC TGG GTC ACG GT) and ferritin–DsRed (sense primer: CGA GAT GAT GTG GCT CTG AA; antisense primer: GAG GAG TCC TGG GTC ACG GT) for 35 cycles (94 °C for 1 min, 55 °C for 1 min, and 72 °C for 2 min) and glyceraldehyde 3 phosphate dehydrogenase, GAPDH (sense primer: TGC ACC ACC AAC TGC TTA G; antisense primer: GAT GCA GGG ATG ATG TTC) for 30 cycles, respectively. The PCR products were resolved by electrophoresis on 2% agarose gels stained with ethidium bromide, then photographed using Light Capture (ATTO Corporation, Tokyo, Japan).

Western blotting. Electroporated G261 cells (1×10^6 cells) were lysed on ice in 100 μl TNE buffer (10 mM Tris–HCl, pH 7.5, 1% NP-40, 0.15 M NaCl, 1 mM EDTA, 10 μg/ml approtinin, 10 μg/ml leupeptin), and sonicated before BCA protein quantification (Pierce, Rockford, IL, USA). Samples of equal protein quantity were separated on 12.5% SDS–PAGE gels and transferred to nitrocellulose membranes for Western blotting according to the iBlot gel transfer system (Invitrogen). To detect DsRed, we used anti-DsRed polyclonal rabbit antibody (CLONTECH Laboratories, Inc., 1:1000 dilution) and ECL plus detection system (GE Healthcare UK Ltd., Buckinghamshire, England). The same membrane was re-probed by anti-GAPDH monoclonal antibody and ECL plus detection took place after detection of DsRed.

FACS analysis. Fluorescence of DsRed in electroporated GL261 cells was analyzed using a FACSCalibur cell sorter (BD Bioscience, San Jose, CA, USA) equipped with a 530 nm filter (bandwidth ± 15 nm) and a 585 nm filter (bandwidth ± 21 nm) and CellQuest software (BD Bioscience).

Brain tumor model. Viable cells were counted using a hemocytometer, and the concentration was adjusted to 5×10^5 cells/5 μl of PBS. Each C57BL/6 mouse was anesthetized and placed in a stereotactic frame, then the skull was exposed. One millimeter of burr holes were drilled and the following coordinates were used to position the 10 μl Hamilton syringe, placing the needle 4.0 mm anterior to the bregma, 4.0 mm lateral to the midline, and 3.5 mm ventral to the cortical surface to deliver cells into the striatum. At each site, an injection volume of 5 μl was delivered at a rate of 1 μl/min, and the needle was withdrawn after an additional 5 min. At 3 weeks after injection, the hearts of anesthetized mice were perfused with about 100 ml isotonic saline, and then each brain was isolated, frozen in liquid nitrogen, and embedded in an OCT compound (Tissue Tek; Miles, Elkhart, IN, USA). In some cases, permeated cells by sonication for 1 min on ice were injected stereotactically into the brain, and the brain was similarly embedded after *in vivo* imaging.

Magnetic resonance imaging (MRI). Mice transplanted GL261 cells were anesthetized with 1.0% isoflurane and held in an MRI coil. It was set on MRI equipment (MRTechnology, Inc., Tsukuba, Japan) and T1 and T2-weighted images were acquired according to the manufacturer's procedure. Recombinant ferritin–DsRed from *Escherichia coli* or GL261 cells were collected in 1.5 ml tubes, and T1 and T2-weighted images were acquired by similar procedure.

Optical imaging. Anesthetized mice were observed using a Maestro (Cambridge Research & Instrumentation, Inc., MA, USA) *in vivo* imaging system equipped with LCTF (Liquid Crystal Tunable Filter), which was useful for spectral analysis between DsRed and autofluorescence. Coronal brain sections were also observed using Maestro, and DsRed-specific fluorescence was detected.

Immunohistochemical staining and Berlin blue staining. Coronal sections (8 μm) of the brains were cut with a cryostatmicrotome, transferred to a MAS coated slide glass (Matsunami Glass Ind., Ltd., Osaka, Japan) and immediately air-dried. Following fixation with 4% paraformaldehyde in PBS (pH 7.2) at room temperature for 10 min, sections were incubated in a blocking buffer (1% bovine serum albumine, 10% normal goat serum, and 0.01% sodium azide) for 30 min at room temperature and labeled with polyclonal antibodies against DsRed at a dilution of 1:500 for 1 h at room temperature. Then sections were visualized with Cy2-conjugated goat anti-rabbit IgG (Rockland Immunochemicals, Inc., Gilbertsville, PA, USA) and counterstained with Hoechst 33342 (Invitrogen, Carlsbad, CA, USA). Several sections were stained with Berlin blue staining. In brief, sections were fixed with ethanol at room temperature for 10 min and washed three times with PBS. The sections were incubated in a mixture of 2% potassium ferrocyanide solution with 1% HCl in equal amounts for 20 min at room temperature and counterstained with Kernechtrot solution (Muto Pure Chemicals Co. Ltd., Tokyo, Japan). Photographs of these sections were then taken under a fluorescent microscope (BX-50, Olympus, Tokyo, Japan).

Image analysis. Images acquired from optical imaging and from MRI were analyzed using Maestro software (Cambridge Research & Instrumentation, Inc.) and Image-Pro Plus software (Roper Industries, Inc., Sarasota, FL, USA), respectively.

Results

Some GL261 cells expressed DsRed at 24 h after electroporation, and the transformants expressing ferritin–DsRed were concentrated by G418 selection (Fig. 1A). FACS analysis showed that ferritin–DsRed-expressing GL261 cells had lower fluorescence compared to DsRed only expressing cells (Fig. 1B). To confirm transgene expression, mRNA expression of DsRed and ferritin–DsRed was analyzed by RT-PCR (Fig. 1C). GL261 cells, electroporated with pferritin–DsRed vectors, were positive for mRNA of both heavy chain of ferritin and DsRed. In addition, analysis by Western blotting indicated existence of ferritin–DsRed fusion protein in lysates from GL261 cells electroporated with pferritin–DsRed vectors (Fig. 1D). To determine whether ferritin–DsRed fusion protein in GL261 cells served as an MRI reporter, the cell pellet (Fig. 2A) was analyzed by T1-weighted images and T2-weighted images (Fig. 2B), since T1-weighted images are generally useful in investigating anatomical structures and T2-weighted images are effective in finding lesion sites in tissues by increasing the signal intensity. T2-weighted images are also highly effective in visualizing existence of iron in high T2-weighted signal intensity in animal tissues. As the first step to examination, we examined recombinant ferritin–DsRed fusion protein from *E. coli* using MRI. In general, T2-weighted images from proteinous pellets (data not shown) or cell pellets (Fig. 2B; middle) in aqueous liquid showed high intensity, however, we found that T2-weighted images from recombinant ferritin–DsRed indicated enhanced visualizing effect by reduction of T2-weighted signal intensity; dense deposits were observed at a site of a pellet (Fig. 2B; top). As the following step, cell pellets from ferritin–DsRed-expressing GL261 cells were observed using

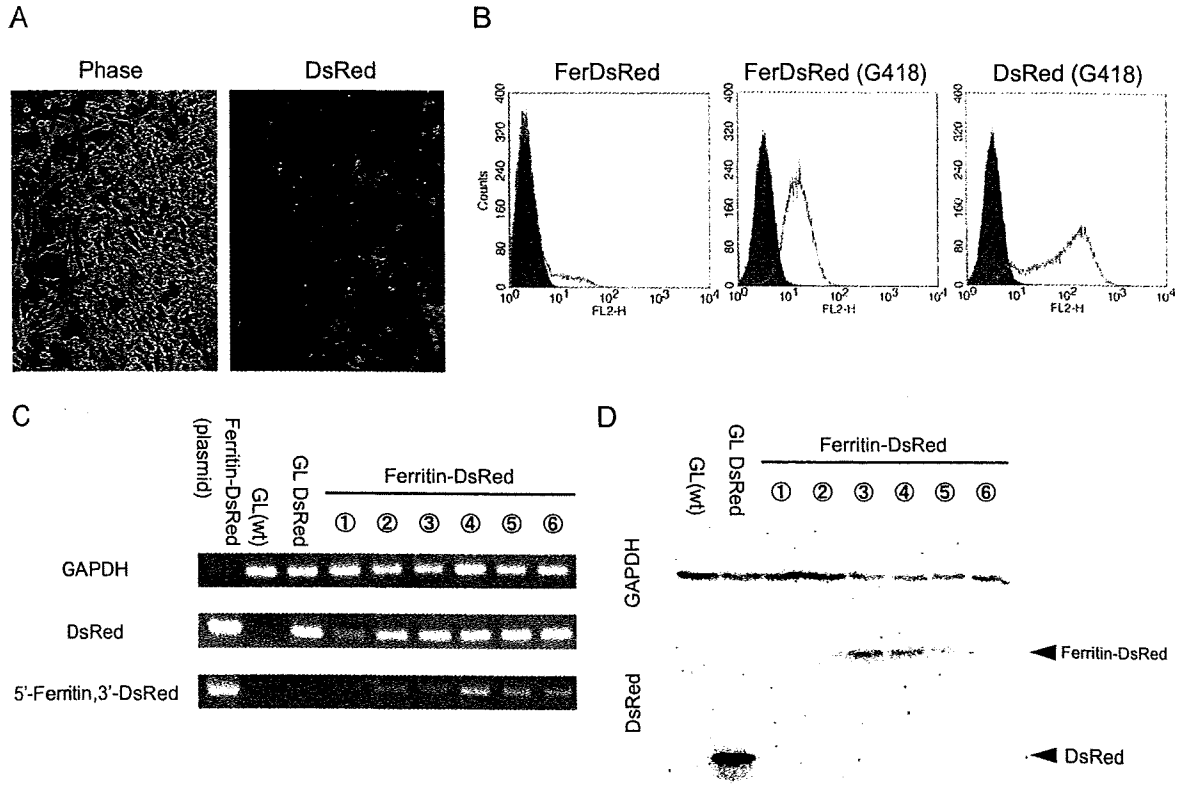

Fig. 1. Production of ferritin–DsRed-expressing GL261 cells. Photographs of ferritin–DsRed-expressing GL261 cells were taken after G418 selection (A). DsRed fluorescence intensity of electroporated GL261 cells was analyzed by FACS (B). The solid line in the left histogram indicated ferritin–DsRed-expressing GL261 cells before G418 selection, the solid line in the center histogram indicated ferritin–DsRed-expressing GL261 cells after G418 selection, and solid line in the right histogram indicated DsRed-expressing GL261 cells after G418 selection. A filled histogram in each histogram indicated GL261 cells. Gene transfer and expression for ferritin–DsRed was confirmed by RT-PCR (C) and Western blotting (D). Ferritin–DsRed (protein); recombinant ferritin–DsRed fusion protein from *E. coli*, GL (wt); GL261 cells, GL DsRed; DsRed expressing GL261 cells after G418 selection, Circle 1; ferritin–DsRed-expressing GL261 cells before G418 selection, Circle 2–6 ferritin–DsRed-expressing GL261 cells after G418 selection.

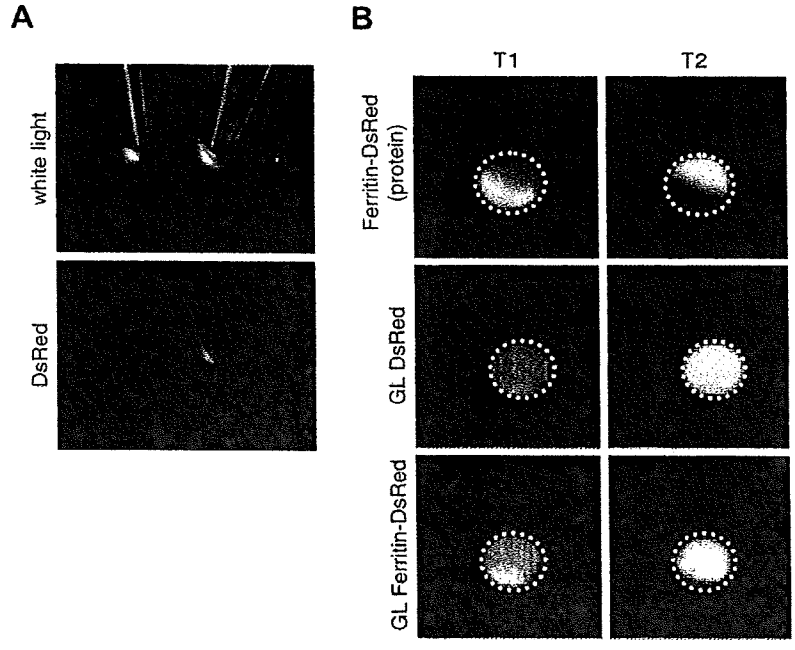

Fig. 2. In vitro optical imaging and MRI of ferritin–DsRed-expressing GL261 cells. Cell pellets from GL261 cells were observed by optical imaging (A) and MRI (B). (A) Left tube was from GL261 cells and right tube was from ferritin–DsRed-expressing GL261 cells. The upper panel indicated a photo exposed to white light and lower panel indicated DsRed fluorescence at the same location. (B) Recombinant protein and cell pellets were acquired for T1-weighted images and T2-weighted images by MRI. Ferritin–DsRed (protein); recombinant ferritin–DsRed fusion protein from *E. coli*, GL DsRed; DsRed-expressing GL261 cells, GL ferritin–DsRed; ferritin–DsRed-expressing GL261 cells, T1; T1-weighted image, T2; T2-weighted image.

MRI. The T2-weighted images indicated a similar dense deposit which meant there was enhanced visualizing effect by reduction of T2-weighted signal intensity for the cell pellet, as ferritin–DsRed fusion protein, but not DsRed expressing GL261 cells. Thus, ferritin expression in GL261 cells was detectable by *in vitro* MRI.

To visualize the reporter transgene expression by *in vivo* MRI, we made a brain tumor model with GL261 cells expressing ferritin–DsRed. At 3 weeks after injection of GL261 cells, mice were analyzed by optical imaging (Fig. 3A). DsRed fluorescence was detected on the right side of the brain, where ferritin–DsRed-expressing GL261 cells were injected. Then, we tried to detect ferritin–DsRed-expressing GL261 cells in the mouse brain, by MRI (Fig. 3B). As the first step to examination, MRI was used to examine a mouse injected with recombinant ferritin–DsRed on the right hemisphere of brain and control protein on the left hemisphere of brain. The T2-weighted images showed a dense core on the right hemisphere due to reduced T2-weighted signal intensity, but no change of signal for the left hemisphere, indicating recombinant ferritin–DsRed could be detected *in vivo*. As a following step, mouse injected with ferritin–DsRed-expressing GL261 cells on the right hemisphere of brain and GL261 cells on the left hemisphere of brain, was observed by MRI. At 3 weeks after injection of GL261 cells, the brain in the T2-weighted image apparently acknowledged for growth of glioma cells, because brain tumors from GL261 cells in the brain increased T2-weighted signal intensity. Photographs of the brain section from the sacrificed mouse were taken and analyzed at the same location of the T2-weighted image (Fig. 3C). The image acquired was fluorescent at the left and right hemispheres of the brain, however, DsRed-specific fluorescence was spectrometrically detected only on the right hemisphere of the brain (Fig. 3C). Since DsRed fluorescence arose from the transplanted GL261 cells expressing ferritin–DsRed, it was confirmed that a dense deposit located around the center of tumor originated from the signal of ferritin–DsRed-expressing cells (Fig. 3D). This was confirmed by a densitometric analysis (Fig. 3D).

Upon preparing the plasmid to express a ferritin reporter for the intracellular domain, we examined whether permeability of iron against plasma membrane affected contrast effects according to ferritin reporter. When permeated ferritin–DsRed-expressing cells were injected into the brain, the contrast was enhanced in T2-weighted images at injected sites, compared to injection of non-permeated cells (Fig. 4A). The immunohistochemical analysis detected many DsRed expressing GL261 cells where the dense deposits were located in the T2-weighted image (Fig. 4B). In

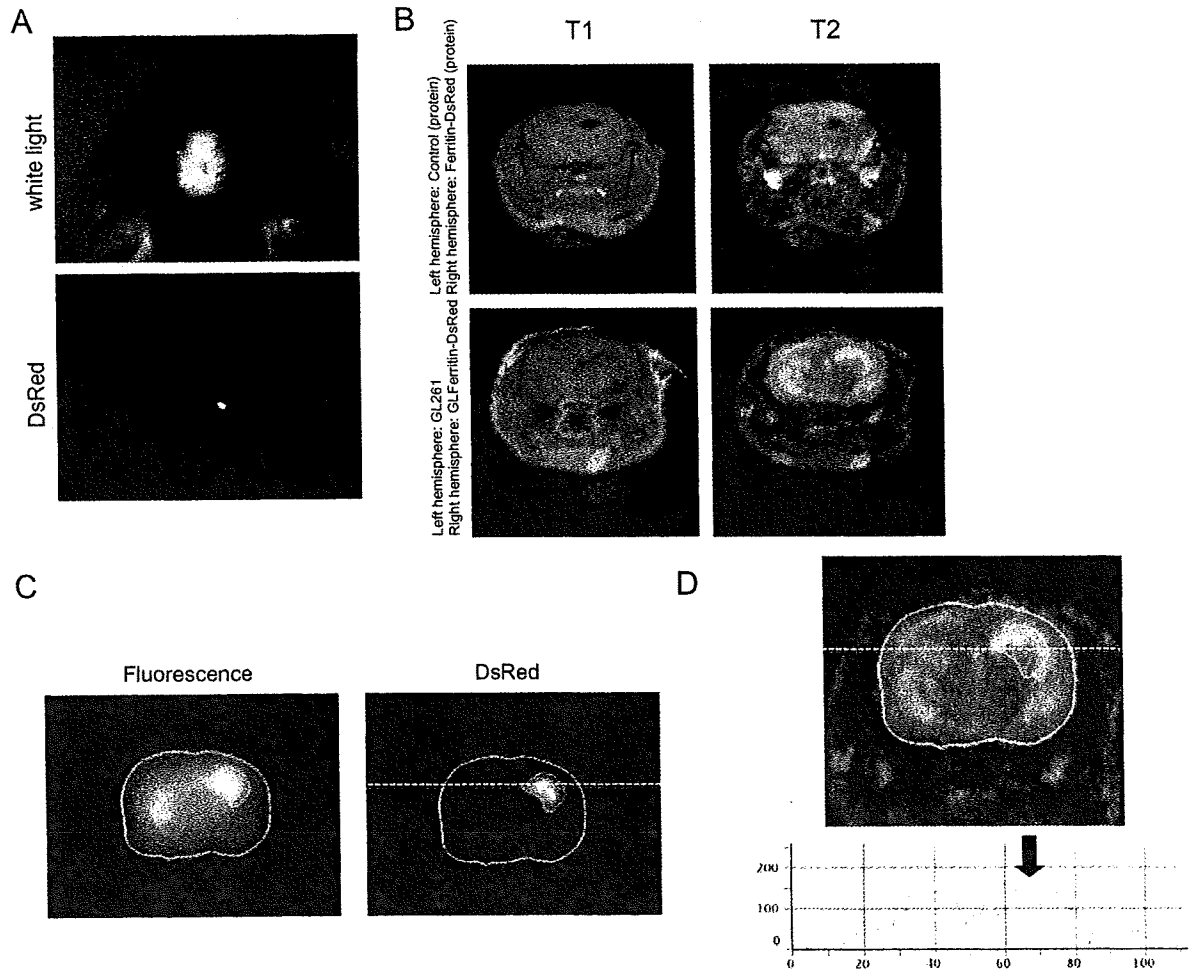

Fig. 3. *In vivo* optical imaging and MRI for ferritin–DsRed-expressing GL261 cells in the brain tumor model. Mouse brain transplanted GL261 cells, were observed by optical imaging (A) and MRI (B). (A) Upper panel indicates a photo exposed to white light and lower panel indicates DsRed fluorescence at the same location. (B) Upper panels showed T1-weighted and T2-weighted images in the brain just after injection of control protein (Left brain) and recombinant ferritin–DsRed (Right brain), and lower panels showed the images in the brain at 3 weeks after injection of control GL261 cells (Left brain) and ferritin–DsRed-expressing GL261 cells (Right brain). A brain section (C) was observed by optical imaging in the same location as MRI images in B. The outline of the brain section and the edge of brain tumor from ferritin–DsRed-expressing GL261 cells was drawn with a white solid line. (D) T2-weighted image (shown in B) overlaid with the white solid line (shown in C). The histogram showed signal intensity with a white dashed straight line in the T2-weighted image and the arrow indicated intensity reduced due to ferritin effect.

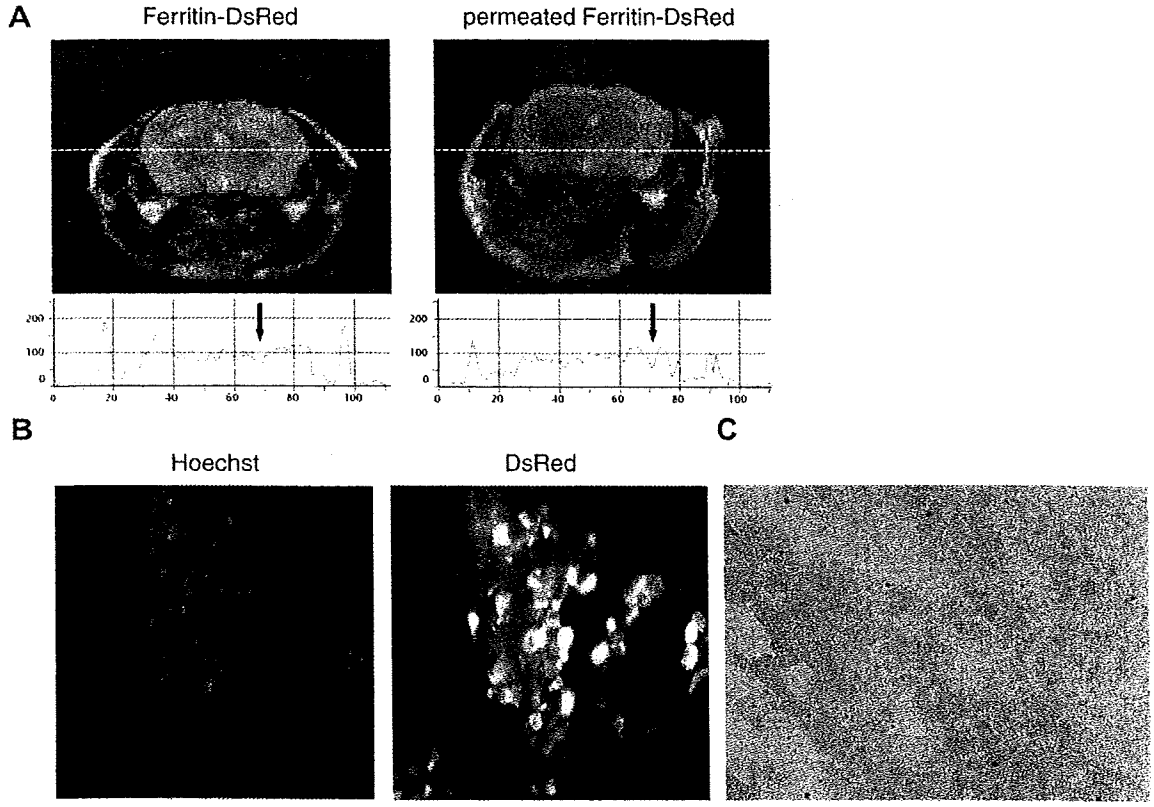

Fig. 4. Contrast effect of ferritin reporter in MRI when membrane permeability of GL261 cells increased. T2-weighted images were shown in (A) when ferritin–DsRed-expressing GL261 cells or the permeated GL261 cells were injected into the mouse right brain. Histograms showed signal intensity on the white dashed straight line and the arrow indicated location of injected GL261 cells. Brain sections from mice injected with permeated cells, were confirmed of DsRed expression (B) by immunohistochemical staining and iron binding (C) by Berlin blue staining.

addition, a lot of iron molecules were located in these cells in brain parenchyma (Fig. 4C).

Discussion

Common consensus was that it was difficult to detect change in gene expression using MRI, as compared to optical imaging. This is because optical imaging using fluorescent protein, such as GFP and DsRed or chemiluminescence with luciferase enzymes, was the common choice. In this study, we particularly focused on the iron effect of reducing the high T2-weighted signal intensity of normal tissue in MRI [2], and studied ferritin molecules where one molecule can bind to 4500 iron atoms at maximum [7]. We successfully chased gene-transfected cells in the brain in our MRI studies using ferritin molecules as a reporter under β-actin promoter control. Since it is easy to convert DsRed to other proteins, this system will be able to chase many protein expressions for both *in vitro* and *in vivo* MRI studies. In addition, this reporter system can also be applied for various cells since the promoter region also changed from a β-actin promoter to other gene promoters, and ferritin molecules can be expressed in intracellular organelles and plasma membranes, as well as cytoplasm.

This study demonstrated that it was possible to visualize gene expression in T2-weighted images for MRI by reducing the high T2-weighted signal intensity in animal tissues with intracellular expression of ferritin. In addition, it was found that there was higher cell permeation against iron enhanced visualizing effect of ferritin, compared to non-permeated cells. This suggests it may be possible to achieve more significant signal visualizing effect, by creating a microenvironment where iron atoms and ferritin molecules can easily bind. Transferrin receptors play an important role in transporting iron from extracellular fluid to intracellular fluid [10]. Therefore, co-expression of transferrin receptors with ferritin molecules may efficiently be improved by reducing signal intensity in T2-weighted images for MRI. Morever, it may be possible to effectively improve visualizing effect with ferritin expression in the extracellular domain of the plasma membrane, instead of the cytoplasm. When compared to the DsRed expressing GL261 cells as a control, we found that ferritin–DsRed-expressing GL261 cells showed low or medium DsRed fluorescence. This indicates that ferritin–DsRed fusion protein expression is less than DsRed. However, it is still unknown whether the expression level is lower due to fusion protein molecular weight or structure that may have affected stability and/or toxicity. Since other studies have reported that overexpression of ferritin alleviated cell damage [11,12], it may not be about cytotoxicity. Further studies will clarify stability and cytotoxicity of over-expressed ferritin molecules.

MRI is a useful and safe clinical diagnostic tool since it doesn't use radiation to get high resolution tomographic images. MRI is also used to monitor blood flow rate with fMRI [13] or gadolinium contrast reagents [14], however, it has not been a technique useful for gene expression imaging. This was due to lack of precise reporters to chase protein expression of the gene expression [15]. Based on our results, use of the ferritin reporter system is expected to expand possibilities to diagnose gene expression using MRI.

Acknowledgments

This study was supported by the Research for Promoting Technological Seeds from Japan Science and Technology Agency and Indus-

trial Technology Research Grant Program from the New Energy and Industrial Technology Development Organization (NEDO) of Japan.

References

[1] G.D. Luker, K.E. Luker, Optical imaging: current applications and future directions, J. Nucl. Med. 49 (2008) 1–4.
[2] J.T. Ferrucci, D.D. Stark, Iron oxide-enhanced MR imaging of the liver and spleen: review of the first 5 years, Am. J. Roentgenol. 155 (1990) 943–950.
[3] R.A. Panizzo, P.G. Kyrtatos, A.N. Price, D.G. Gadian, P. Ferretti, M.F. Lythgoe, In vivo magnetic resonance imaging of endogenous neuroblasts labelled with a ferumoxide–polycation complex, Neuroimage 44 (2009) 1239–1246.
[4] K. Imam, D.A. Bluemke, MR imaging in the evaluation of hepatic metastases, Magn. Reson. Imaging Clin. N. Am. 8 (2000) 741–756.
[5] S. Hirohashi, H. Uchida, K. Yoshikawa, N. Fujita, K. Ohtomo, Y. Yuasa, Y. Kawamura, O. Matsui, Large scale clinical evaluation of bowel contrast agent containing ferric ammonium citrate in MRI, Magn. Reson. Imaging 12 (1994) 837–846.
[6] B. Cohen, K. Ziv, V. Plaks, T. Israely, V. Kalchenko, A. Harmelin, L.E. Benjamin, M. Neeman, MRI detection of transcriptional regulation of gene expression in transgenic mice, Nat. Med. 13 (2007) 498–503.
[7] E.C. Theil, Ferritin: at the crossroads of iron and oxygen metabolism, J. Nutr. 133 (2003) 1549S–1553S.
[8] C. Ferreira, D. Bucchini, M.E. Martin, S. Levi, P. Arosio, B. Grandchamp, C. Beaumont, Early embryonic lethality of H ferritin gene deletion in mice, J. Biol. Chem. 275 (2000) 3021–3024.
[9] Z. Gottesfeld, M. Neeman, Ferritin effect on the transverse relaxation of water: NMR microscopy at 9.4 T, Magn. Reson. Med. 35 (1996) 514–520.
[10] A.E. Deans, Y.Z. Wadghiri, L.M. Bernas, X. Yu, B.K. Rutt, D.H. Turnbull, Cellular MRI contrast via coexpression of transferrin receptor and ferritin, Magn. Reson. Med. 56 (2006) 51–59.
[11] M. Festa, G. Ricciardelli, G. Mele, C. Pietropaolo, A. Ruffo, A. Colonna, Overexpression of H ferritin and up-regulation of iron regulatory protein genes during differentiation of 3T3-L1 pre-adipocytes, J. Biol. Chem. 275 (2000) 36708–36712.
[12] A. Cozzi, B. Corsi, S. Levi, P. Santambrogio, A. Albertini, P. Arosio, Overexpression of wild type and mutated human ferritin H-chain in HeLa cells: in vivo role of ferritin ferroxidase activity, J. Biol. Chem. 275 (2000) 25122–25129.
[13] E.A. DeYoe, P. Bandettini, J. Neitz, D. Miller, P. Winans, Functional magnetic resonance imaging (FMRI) of the human brain, J. Neurosci. Methods 54 (1994) 171–187.
[14] G.L. Wolf, Current status of MR imaging contrast agents: special report, Radiology 172 (1989) 709–710.
[15] R. Weissleder, A clearer vision for in vivo imaging, Nat. Biotechnol. 19 (2001) 316–317.

Ann Nucl Med (2010) 24:163–169
DOI 10.1007/s12149-009-0339-0

ORIGINAL ARTICLE

Two activated stages of microglia and PET imaging of peripheral benzodiazepine receptors with [^{11}C]PK11195 in rats

Fumitaka Ito · Hiroshi Toyama · Gen Kudo · Hiromi Suzuki · Kentaro Hatano · Masanori Ichise · Kazuhiro Katada · Kengo Ito · Makoto Sawada

Received: 2 September 2009 / Accepted: 8 December 2009 / Published online: 26 January 2010

Abstract
Objective The transition of microglia from the normal resting state to the activated state is associated with an increased expression of peripheral benzodiazepine receptors (PBR). The extent of PBR expression is dependent on the level of microglial activation. A PBR ligand, [^{11}C]PK11195, has been used for imaging of the activation of microglia in vivo. We evaluated whether [^{11}C]PK11195 PET can indicate differences of microglial activation between no treatment and lipopolysaccharide (LPS) treatment in a rat artificial injury model of brain inflammation.
Methods On day 1, a small aliquot of absolute ethanol was injected into the rat right striatum (ST) to produce artificial brain injury. On day 3, MRI scans were performed to evaluate and select rats showing a similar degree of brain injury. Then LPS or vehicle was administered intraperitoneally. On day 4, PET scans were performed after a bolus injection of [^{11}C]PK11195. Eleven rats (7 LPS administered rats, 4 LPS non-administered rats) were evaluated. We used uptake ratios of the integral of right and left striatum from 0 to 60 min as an estimate of PBR distribution volume (V_{60}). The number of activated microglia and mRNA expression of inflammatory cytokines (TNFα, IL-1β) were assessed by isolectin-B4 staining and RT-PCR, respectively.
Results Right/left ST V_{60} ratios of LPS group were significantly higher than those of non-LPS group ($P < 0.03$). Although there were no significant differences in the number of activated microglia between the two groups, LPS group showed higher expression of inflammatory cytokines (TNFα, IL-1β) than the non-treated group indicating that further activation was induced by LPS treatment.
Conclusion The results suggest that intensity of PBR signals in [^{11}C]PK11195 PET may be related to the level of microglial activation rather than the number in activated microglia at least in an artificial brain injury model.

Keywords Peripheral benzodiazepine receptor · Animal PET · Activated microglia · Toxic conversion · Lipopolysaccharide

F. Ito (✉) · H. Toyama · G. Kudo · K. Katada
Department of Radiology, Fujita Health University,
1-98 Dengakugakubo, Kutsukake, Toyoake
Aichi 470-1192, Japan
e-mail: fito@fujita-hu.ac.jp

H. Suzuki · M. Sawada
Department of Brain Function,
Research Institute of Environmental Medicine,
Nagoya University, Nagoya, Japan

K. Hatano · K. Ito
Department of Brain Science and Molecular Imaging,
National Institute for Longevity Science, National Center
for Geriatrics and Gerontology, Obu, Japan

M. Ichise
Department of Radiology, Columbia University,
New York, NY, USA

Introduction

Microglia are central nervous system cells having various properties, such as control of neuronal activity and homeostasis, and release of neurotrophic and neurotoxic factors including nitric oxide, cytokines, and neurotrophins. Microglia convert to activated forms when diseases cause neuronal degeneration and the activated microglia accumulate in the affected areas [1], a portion of which proliferates in response to the appropriate intercellular

signaling. Histopathologically, microglial activation begins from several hours and lasts for several days after disease onset [2, 3]; this early microglial activation appears to be an important factor for the formation of various brain lesions seen in several neurodegenerative diseases, brain infarction, and brain tumors. Several lines of evidence suggest that there are some functional differences in activated microglia; some of them indicate cytotoxic properties, which produce several toxic materials to eliminate damaged cells beyond the point of recovery, while others indicate rather protective characteristics, which release neurotrophic factors and protect cells from damage [4, 5]. The former state of activated microglia is sometimes referred to as a 'further activated' or 'fully activated' form. These two different characteristics of activated microglia play an important role in the pathophysiology of common disorders, such as Alzheimer's disease and Parkinson's disease. It is worth distinguishing between the two different activated states of microglia for the diagnosis of brain diseases and possibly for planning further treatment strategies. However, there is no reliable in vivo method to evaluate the contribution of different states of activated microglia to the disease process.

Microglial activation has been shown to increase the expression of peripheral benzodiazepine receptors (PBR) that are located on the mitochondrial membrane of the microglia [6]. PBR is a widely distributed transmembrane protein that is located mainly in the outer mitochondrial membrane. Many functions are associated with the PBR, including regulation of cholesterol transport and synthesis of steroid hormones, porphyrin transport, and heme synthesis. Recently, PBR has been renamed as "translocator protein (18 kDa)" due to recent data regarding the structure and molecular function of this protein [7].

[^{11}C]PK11195 is a PET radioligand used to image PBR. This ligand can be easily labeled with a positron emitter, crosses the blood-brain barrier and binds reversibly to the central PBR. However, because of relatively low affinity of [^{11}C]PK11195 for PBR [8–10], the target to background ratio is relatively low [11] compared to newly developed ligands [12–14] and the biological significance of [^{11}C]PK11195 in terms of microglial activation has not been fully investigated. We showed previously that activated microglia in a rat model of brain inflammation induced by ethanol microinjection accumulate in the damaged area and that microglial activation resulted in a significant increase in the [^{11}C]PK11195 signal in vivo [15].

In the present study, we experimentally induced the two different states of activated microglia and evaluated the level of activated states with [^{11}C]PK11195 PET imaging of PBR in rats.

Materials and methods

The experimental procedures are described in chronological order as below.

Animal model preparation

All procedures were conducted in accordance with the guidelines of the National Institutes of Health and Animal Experimentation of Fujita Health University, School of Medicine. The study protocol was approved by the Animal Experimentation Ethics Committee of the National Center for Geriatrics and Gerontology.

Using 9-week-old male Wistar rats weighing 280–300 g (Nihon Charles River, Tokyo, Japan), general anesthesia was induced by administering pentobarbital (50 mg/kg). After immobilizing the head using a brain stereotactic apparatus (Narishige, Tokyo, Japan), an incision was placed on the scalp to expose the skull. Using a bone drill, a hole was made in the skull to an area that was 0.4 mm anterior, 3 mm lateral, and 4.5 mm ventral to the bregma (point on the skull where the coronal and sagittal sutures converge), and using a 10-μl Hamilton syringe, 8 μl of ethanol was injected to the right striatum to cause brain injury [3].

MRI imaging

After preparing the artificial brain injury model, stereotactic MRI imaging was performed to identify the location of the brain injury, and the severity of the brain injury in the rat striatum was assessed on T1-weighted, T2-weighted, and Gd-DTPA enhanced T1-weighted images. Gd-DTPA enhanced T1-weighted images were used to confirm the presence or absence of the destruction of the blood-brain barrier due to ethanol injection to the right striatum.

We performed the following PET scanning with and without LPS injections only for injured rats showing almost the same extent of high intensity area around the ethanol injected right striatum on the T2 weighted images (Fig. 1).

For MRI scanning, the Signa Infinity Excite (1.5 T, GE Healthcare, Milwaukee, USA) and a wrist coil (Q-WRIST, GE Healthcare, Milwaukee, USA) were used.

LPS treatment

Just after the MRI scanning, to induce further activation of microglia, LPS (SIGMA-ALDRICH, Saint Luis, USA) was injected intraperitoneally (10 mg/kg) to seven out of eleven rats (LPS group), and vehicle was injected to the others (non-LPS group).

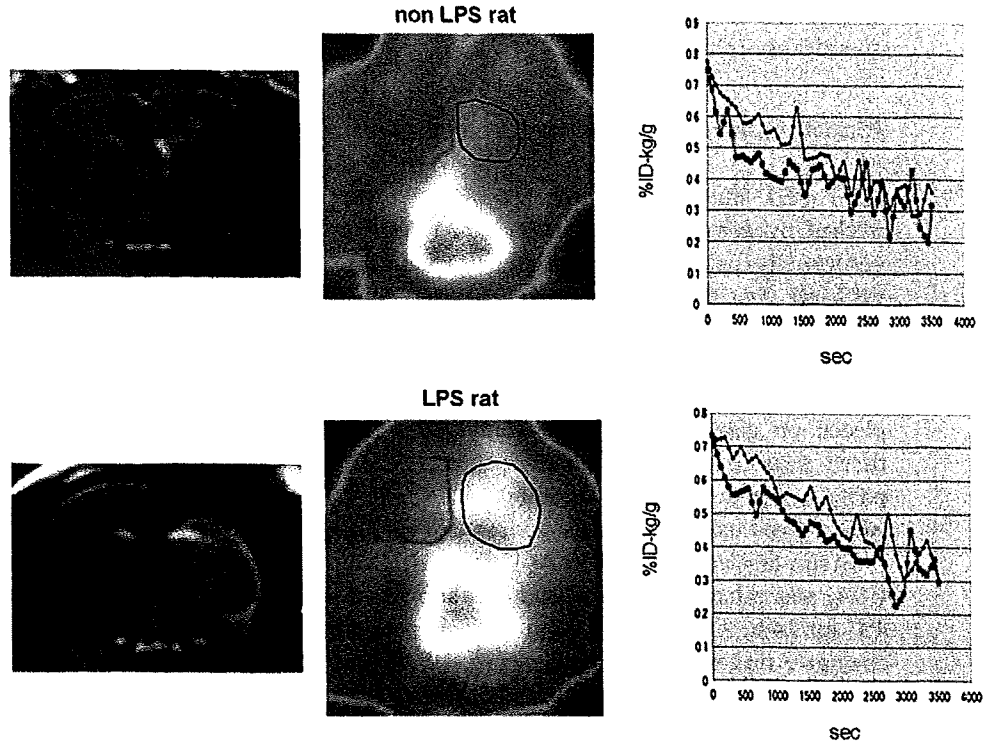

Fig. 1 Representative coronal MRI T2 weighted images (*left column*), summed images (0–60 min) and time-activity curves (injured right and non-injured left striatum) of [^{11}C]PK-11195 in ethanol injury rats for a non-LPS rat (*upper row*) and an LPS rat (*lower row*). The ROIs are placed in bilateral striata on the [^{11}C]PK-11195 images. *Blue lines* show injured right striatum and *pink lines* show non-injured left striatum. LPS rat shows much slower clearance in injured right striatum as compared with non-injured left striatum than in non-LPS rat

PET imaging

Using the method reported by Sakiyama et al. [16] and our group [15], anesthesia was induced by intraperitoneally administering chloral hydrate (300 mg/kg), and the head of each rat was fixed using an acrylic brain stereotactic device (Hamamatsu Photonics, Hamamatsu, Japan). To prevent anesthesia-induced hypothermia, a heat mat was placed under the rat to maintain its rectal temperature at 37.0 ± 0.5°C. PET was performed using an animal PET scanner (SHR-2000, Hamamatsu Photonics, Hamamatsu, Japan, spatial resolution: 3.5 mm FWHM). Under general anesthesia induced by infusing chloral hydrate through the tail vein (100 mg/kg/h), 39–64 MBq of [^{11}C]PK11195 was administered intravenously as a bolus, and PET was immediately performed for 60 min (1 min/frame).

PET data analysis

PET images were analyzed using our previously reported method [15]. With small rat brain and limited number of voxels involved, rather than cluster analysis as used by the Hammersmith hospital group [17–19] or reference tissue models [20, 21], we sought to estimate a more direct measure of PBRs receptor binding by an ROI-based approach to estimate the distribution volume.

Based on our previously reported method [15], regions of interest (ROIs) were established on the cross-sectional stereotactic [^{11}C]raclopride PET image which was performed previously for template at the level of the bilateral striata. Guided by these [^{11}C]raclopride striatal ROIs, ROIs were placed for the bilateral striata on stereotactic [^{11}C]PK11195 PET images.

As reported previously [15], PBR binding was estimated by calculating the ipsi- to contra-lateral area ratio of the time-activity curve (TAC).

Intracerebral distribution volume (V) was defined as follows [22]:

$$V = \frac{\int_0^{\infty} \mathrm{ROI}\, dt}{\int_0^{\infty} \mathrm{Plasma}\, dt}.$$

In this study, V was approximated as the area under the curve (AUC) ratio from minutes 0 to 60 min (V_{60}).

The ratio of the V_{60} for the right striatum with brain injury (RST) to that for the left striatum without injury (LST) was calculated as follows:

$$V_{60}\,(\mathrm{RST})/V_{60}(\mathrm{LST}) = (\mathrm{RST\ AUC/plasma\ AUC})/(\mathrm{LST\ AUC/plasma\ AUC}) = \mathrm{RST\ AUC/LST\ AUC}.$$

The calculation of the above V_{60} ratios actually did not require plasma data because the plasma AUC term cancels out in the above equation. An unpaired t test was used to

compare the LPS and non-LPS groups with the level of significance set at $P < 0.05$.

Histochemical assessment of activated microglia

After PET imaging, additional anesthesia was accomplished by administering pentobarbital (50 mg/kg) intraperitoneally, and after transcardial perfusion using 0.01 M PBS (pH: 7.4), the brain tissue was removed. Excised fresh brain tissue was mounted using an OCT compound (Dako Cytomation, Carpinteria, USA) and quickly frozen, and then 10-μm sections were prepared using a cryostat and placed on gelatin-coated slide glass. After fixing brain tissue sections using 4% paraformaldehyde/0.1 M phosphate buffer at room temperature for 10 min, microglia were stained using biotin-labeled isolectin-B4 (IB4) [23].

Biotin-labeled IB4 (SIGMA-ALDRICH, Saint Louis, USA) was diluted to 2 μg/μl and was allowed to react at 4°C for 24 h. After washing with PBS, streptoavidin–HRP conjugate reagent (KPL, Gaithersburg, USA) was labeled at room temperature for 30 min, and 3,3′-diaminobenzidine tetrahydrochloride (DAB, Vector Lab., Burlingame, USA) was used for the detection at room temperature for 10 min. After DAB, hematoxylin was used for nuclear staining.

After staining, a virtual microscope Aperio (Aperio Technologies, Viata, USA, microscope-incorporated line-scan slide glass scanner) was used to histologically quantify the number of IB4-positive activated microglia in the left and right striata with ImagePro software which allows automatic threshold setting in relation to background data. For each rat, the results of five sections were averaged. An unpaired t test was used to compare the LPS and non-LPS groups with the level of significance set at $P < 0.05$.

Evaluation of the extent of microglial activation by examining the inflammatory cytokines

Using adjacent frozen brain sections to the sections used in immunohistological analysis, total RNA was extracted to assess the mRNA expression of inflammatory cytokines, TNFα, and Il-1β, by RT-PCR for a marker of activated microglia. Rat brain tissue was sliced into 10-μm sections, and 15 sections were placed in 1.5-ml plastic tubes. Lysis buffer composed of RLT buffer and 2-mercaptoethanol (B-ME, SIGMA-ALDRICH, Saint Louis, USA) was added, and the tissue sections were crushed. The RNeasy total RNA isolation kit (QIAGEN, Valencia, USA) was used for RNA extraction, and using 1 μg of total RNA, RT-PCR was performed using the previously reported method [24]. After PCR, products were analyzed by electrophoresis using ethidium bromide stained 2% agarose gel, and then quantified with ATTO coolserver software (ATTO, Tokyo, Japan).

Results

Histochemical assessment of activated microglia by comparison of numbers of activated microglia between injured and non-injured striata

When compared to the non-injured left striatum, IB4-positive activated microglial accumulation was observed around the injured right striatum, and activated microglia exhibited an ameboidal shape (Fig. 2). Marked tissue loss was seen in the injured striatum for the LPS group (Fig. 3-1) suggesting that further activation of microglia was induced by LPS treatment. However, both with and without LPS administration, numerous ameboidal shape IB4-positive microglia were observed in injured striatum (Fig. 3-1), and there were no significant differences in the number of IB4-positive activated microglia between the two groups (Fig. 3-2).

Assessment of the level of microglial activation by inflammatory cytokine expression

The amount of expression of inflammatory cytokine mRNA is dependent on the extent of activated microglia. So, TNFα and IL-1β mRNA expression was compared between the LPS and non-LPS groups. The expression of TNFα and IL-1β in the LPS rats was greater (Fig. 4-1) than that in the non-LPS treated rats.

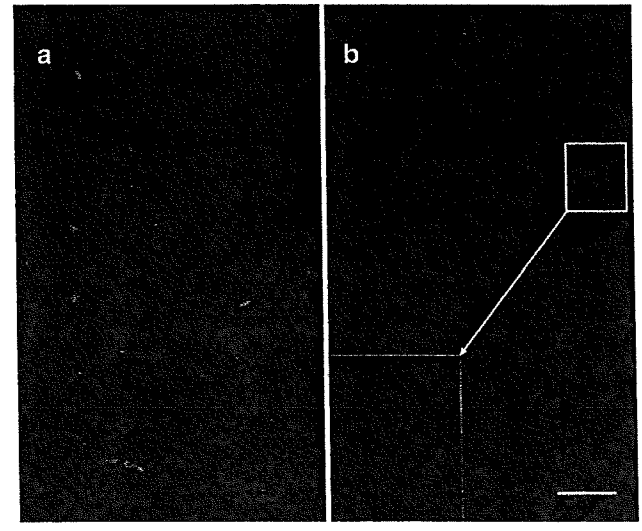

Fig. 2 Immunohistochemical staining (Isolectin-B4 stain) on the ethanol-injured right and non-injured left striatum in the same lesioned rat model (*Bar* 10 μm). Microglial accumulation is not seen in non-injured striatum (a). Ameboidal activated microglial accumulation is seen around the injured striatum (b)

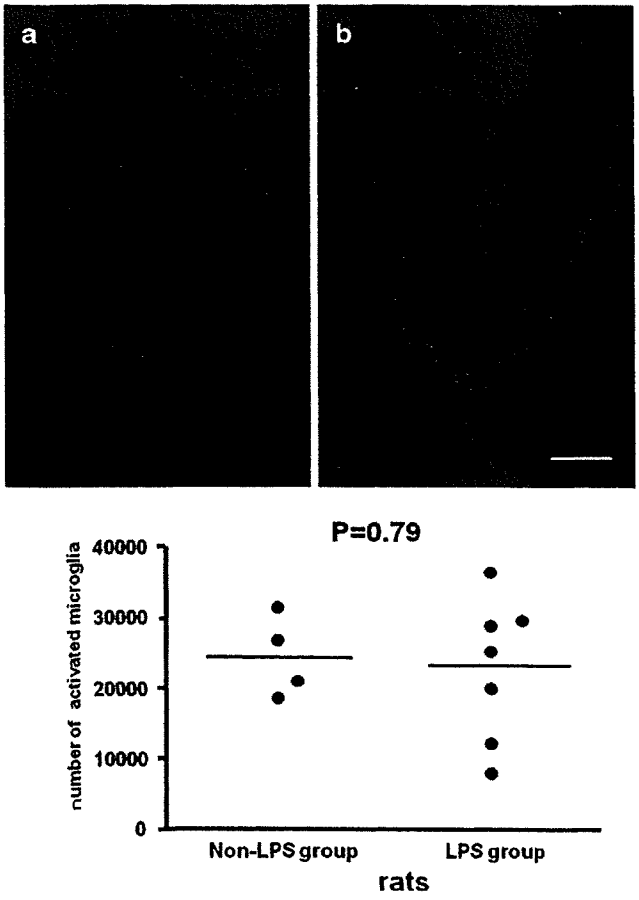

Fig. 3 1 Effects of intraperitoneal LPS administration on the ethanol injury model. When compared to the non-LPS rat (a), marked tissue loss is seen in the LPS rat (b), and microglial accumulation is seen around the ethanol-injured striatum. Isolectin-B4 was used for histological staining (*Bar* 10 μm) 2 Comparison of number of activated microglial cells in the injured striatum of the ethanol injury model between LPS and non-LPS group. No significant differences are seen in the number of activated microglial cells between the two groups

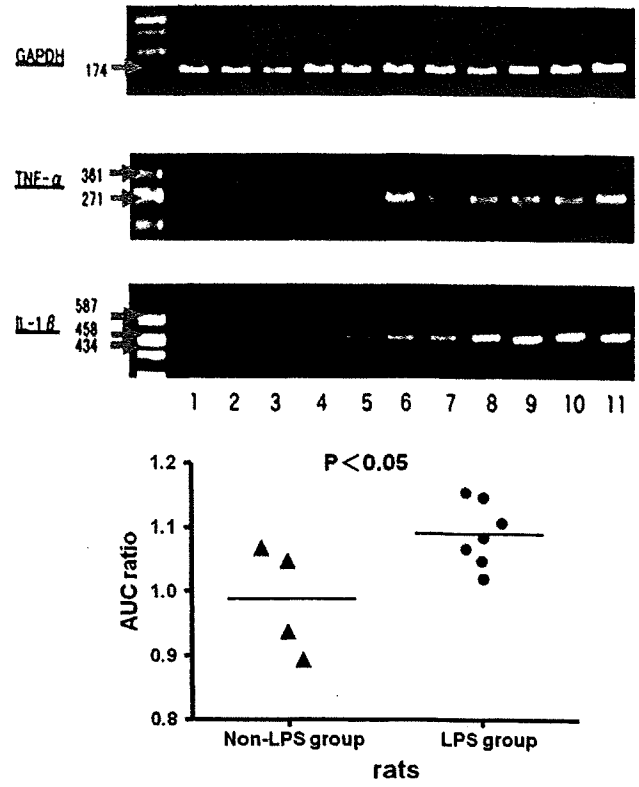

Fig. 4 1 Expression of inflammatory cytokines in the ethanol injury model. All LPS group rats show intense increased expressions both in TNFα and in IL-1β (*lanes 5–11*). However, non-LPS group rats show mildly increased expression both in TNFα and in IL-1β (*lanes 1–4*). TNFα rat primer: product size 289 Fw5′-GCCTCAGCCTCTTCT GAT-3′, Bw5′-ACCAGTTGGTTGTCTTTG-3′, IL-1β rat primer: product size 467, Fw5′-CGACAGTGAGGAGAATGA-3′, Bw5′-CGTTGCTTGTCTCTCCTT-3′, GAPDH rat primer: product size 174, Fw5′-TGCACCACCAACTGCTTA-3′, Bw5′-GATGCAGGG ATGATGTTC-3′. 2 The ethanol-injured right to non-injured left striatum region ratio of the area under the time-activity curve (AUC) of the ^{11}C-PK11195 dynamic PET. The AUC ratio for the LPS group is significantly greater than that for the non-LPS group

Comparison of PBR signal in [^{11}C]PK11195 PET

The AUC ratio for the LPS group was 1.09 ± 0.05, which was significantly greater than that for the non-LPS group at 0.99 ± 0.05 ($P < 0.05$; Fig. 4-2).

Summed images and time-activity curves of [^{11}C]PK11195 PET in representative LPS and non-LPS rats are shown in Fig. 1.

Discussion

In the present study, we experimentally induced the two different states of activated microglia and evaluated the level of activated states with PET imaging of PBR in rats. We found that intensity of PBR signals in [^{11}C]PK11195 PET may be related to level of microglial activation rather than number in activated microglia at least in an artificial brain injury model.

There was a marked neuronal degeneration for the LPS group around the artificially damaged striatum and activated microglia accumulated around the ipsilateral striatum. Sawada et al. [3] found that intraperitoneal administration of LPS increased the size of artificial injury and the number of damaged nerve fibers around the injury, as detected by FluoroJadeB (unpublished observation). In the brain injury model which we used in this experiment, peripheral inflammatory cells do not contribute to brain inflammation and damage as reported previously. Thus, IB4-positive cells reflect the activation of endogenous microglia in this brain injury model [3]. Therefore, the difference in the histological findings that marked tissue loss was seen in the damaged striatum of the LPS group

should be related to further activation of microglia that were induced by LPS administration.

Hardwick et al. [25] reported the increased [^{11}C]PK11195 accumulation in the lungs of LPS-treated mice on in vivo small animal PET studies. Venneti et al. [26] demonstrated that [^{3}H](R)-PK11195 binding was increased in activated macrophages using post mortem tissues from macaques' encephalitis with simian immunodeficiency virus infection and also macrophage cultures treated with LPS. In this report we indicated that increased [^{11}C]PK11195 uptake in animal PET correlates with the extent of microglial activation in the brain after LPS administration. We observed that LPS administration markedly increased the expression of inflammatory cytokines (Fig. 4-1), indicating that additional activation of microglia was induced by LPS treatment; this state of the activation might be correlated with toxic state of microglial activation since damage severity was marked in LPS-treated brain. It is possible that peripherally administered LPS could activate cerebral microglia to induce the expression of inflammatory cytokines as reported previously [4]. In spite of increase of inflammatory cytokine expression, no significant differences were observed in the total number of activated microglia in the artificially damaged striatum between the LPS and non-LPS groups (Fig. 3-2). These results suggest that LPS administration caused further activation of microglia located at the surrounding area in the injured striatum. Accompanied with the histological observation and PCR analysis, this activated state may relate to the toxic form of activated microglia. We should address that PBR expression is actually amplified by toxic conversion of activated microglia.

Conclusions

The results suggest that intensity of PBR signals in [^{11}C]PK11195 PET may be related to level of microglial activation rather than number in activated microglia at least in an artificial brain injury model.

Acknowledgments We would like to thank Mr. Junichiro Abe, Department of Brain Science and Molecular Imaging, National Institute for Longevity Sciences, National Center for Geriatrics and Gerontology, Obu, Japan for running cyclotron. We appreciate radiological technologists, Fujita Health University Hospital for running the MRI scanner. We also thank Eizou Umezawa, PhD, School of Health Sciences, Fujita Health University for providing support with regard to statistical analysis. This study was supported by Japan Society for the Promotion of Science (JSPS) KAKENHI (18591369, 80001800), the 21st Century COE (Center of Excellence) Medical Program (Development Center for Targeted and Minimally Invasive Diagnosis and Treatment) from JSPS, and a grant from Fujita Health University.

References

1. Kreutzberg GW. Microglia: a sensor for pathological events in the CNS. Trends Neurosci. 1996;19:312–8.
2. Banati RB. Neuropathological imaging: in vivo detection of glial activation as a measure of disease and adaptive change in the brain. Br Med Bull. 2003;65:121–31.
3. Takeuchi A, Isobe K, Miyaishi O, Sawada M, Fan ZH, Nakashima I, et al. Microglial NO induces delayed neuronal death following acute injury in the striatum. Eur J Neurosci. 1998;10:1613–20.
4. Sawada M, Suzumura A, Marunouchi T. Cytokine network in the central nervous system and its roles in growth and differentiation of glial and neuronal cells. Int J Dev Neurosci. 1995;13:253–64.
5. Sawada M, Sawada H, Nagatsu T. Effects of aging on neuroprotective and neurotoxic properties of microglia in neurodegenerative diseases. Neurodegener Dis. 2008;5:254–6.
6. Banati RB, Egensperger R, Maassen A, Hager G, Kreutzberg G, Graeber MB. Mitochondria in activated microglia in vitro. J Neurocytol. 2004;33:535–41.
7. Papadopoulos V, Baraldi M, Guilarte TR, Knudsen TB, Lacapere JJ, Lindemann P, et al. Translocator protein (18 kDa): new nomenclature for the peripheral-type benzodiazepine receptor based on its structure and molecular function. Trends Pharmacol Sci. 2006;27:402–9.
8. Vowinckel E, Reutens D, Becher B, Verge G, Evans A, Owens T, et al. PK11195 binding to the peripheral benzodiazepine receptor as a marker of microglia activation in multiple sclerosis and experimental autoimmune encephalomyelitis. J Neurosci Res. 1997;50:345–53.
9. Debruyne JC, VanLaere KJ, Versijpt J, DeVos F, Eng JK, Strijckmans K, et al. Semiquantification of the peripheral-type benzodiazepine ligand [^{11}C]PK11195 in normal human brain and application in multiple sclerosis patients. Acta Neurol Belg. 2002;102:127–35.
10. Zhang MR, Maeda J, Ogawa M, Noguchi J, Ito T, Obayashi S, et al. Development of a new radioligand, *N*-(5-fluoro-2-phenoxyphenyl)-*N*-(2-[^{18}F]fluoroethyl-5-methoxybenzyl) acetamide, for PET imaging of peripheral benzodiazepine receptor in primate brain. J Med Chem. 2004;47:2228–35.
11. Groom GN, Junck L, Foster NL, Frey KA, Kuhl DE. PET of peripheral benzodiazepine binding sites in the microgliosis of Alzheimer's disease. J Nucl Med. 1995;36:2207–10.
12. Maeda J, Higuchi M, Inaji M, Ji B, Haneda E, Okauchi T, et al. Phase-dependent roles of reactive microglia and astrocytes in nervous system injury as delineated by imaging of peripheral benzodiazepine receptor. Brain Res. 2007;1157:100–11.
13. Venneti S, Lopresti BJ, Wang G, Slagel SL, Mason NS, Mathis C, et al. A comparison of the high-affinity peripheral benzodiazepine receptor ligands DAA 1106 and (R)-PK11195 in rat models of neuroinflammation: implications for PET imaging of microglial activation. J Neurochem. 2007;102:2118–31.
14. Imaizumi M, Kim H-J, Zoghbi SS, Briard E, Hong J, Musachio JL, et al. PET imaging with [^{11}C]PBR28 can localize and quantify upregulated peripheral benzodiazepine receptors associated with cerebral ischemia in rat. Neurosci Lett. 2007;411:200–5.
15. Toyama H, Hatano K, Suzuki H, Ichise M, Momosaki S, Kudo G, et al. In vivo imaging of microglial activation using a peripheral benzodiazepine receptor ligand: [^{11}C]PK-11195 and animal PET following ethanol injury in rat striatum. Ann Nucl Med. 2008;22:417–24.
16. Sakiyama Y, Hatano K, Kato T, Tajima T, Kawasumi Y, Ito K. Stimulation of adenosine A1 receptors decreases in vivo dopamine D1 receptor binding of [^{11}C]SCH23390 in the cat striatum

revealed by positron emission tomography. Ann Nucl Med. 2007;21:447–53.
17. Banati RB. Visualizing microglial activation in vivo. Glia. 2002;40:206–17.
18. Cagnin A, Brooks DJ, Kennedy AM, Gunn RN, Myers R, Turkheimer FE, et al. In vivo measurement of activated microglia in dementia. Lancet. 2001;358:461–7.
19. Gunn RN, Lammertsma AA, Hume SP, Cunningham VJ. Parametric imaging of ligand-receptor interactions using a reference tissue model and cluster analysis. In: Carson R, Daule M, Witherspoon P, Herscovitch P, editors. Quantitative functional brain imaging with positron emission tomography. San Diego: Academic Press; 1998. p. 401–6.
20. Kropholler MA, Boellaard R, Schuitemaker A, Folkersma H, van Berckel BNM, Lammertsma A. Evaluation of reference tissue models for the analysis of [^{11}C](R)-PK11195 studies. J Cereb Blood Flow Metab. 2006;26:1431–41.
21. Schuitemaker A, van Berckel BNM, Kropholler MA, Veltman DJ, Scheltens P, Jonker C, et al. SPM analysis of parametric (R)-[^{11}C]-PK11195 binding images: plasma input versus reference tissue parametric methods. NeuroImage. 2007;35:1473–9.
22. Lassen NA. Neuroreceptor quantitation in vivo by the steadystate principle using constant infusion or bolus injection of radioactive tracers. J Cereb Blood Flow Metab. 1992;12:709–16.
23. Streit WJ. An improved staining method for rat microglial cells using the lectin from Griffonia simplicifonia (GSA I-B4). J Histochem Cytochem. 1990;38:1683–6.
24. Suradhat S, Thanawongnuwech R, Poovorawan Y. Upregulation of IL-10 gene expression in porcine peripheral blood mononuclear cells by porcine reproductive and respiratory syndrome virus. J Gen Virol. 2003;84:453–9.
25. Hardwick MJ, Chen MK, Baidoo K, Pomper MG, Guilarte TR. In vivo imaging of PBRs in mouse lungs: a biomarker of inflammation. Mol Imaging. 2005;4:432–8.
26. Venneti S, Wang G, Wiley CA. Activated macrophages in HIV encephalitis and a macaque model show increased [^{3}H](R)-PK11195 binding in a PI3-kinase-dependent manner. Neurosci Lett. 2007;426:117–22.